DESIGN, MICROFABRICATION AND CHARACTERIZATION OF A MICROHEATER PLATFORM FOR STUDYING DNA-SURFACE INTERACTIONS

by

ANNAS JAVED

Presented to the Faculty of the Graduate School of

The University of Texas at Arlington in Partial Fulfillment

of the Requirements

for the Degree of

MASTER OF SCIENCE IN ELECTRICAL ENGINEERING

THE UNIVERSITY OF TEXAS AT ARLINGTON

May 2012

ACKNOWLEDGEMENTS

All praises and thanks to the God Almighty for without His blessings and guidance nothing is possible.

I would like to thank Dr. Ankur Jain for giving me such a wonderful opportunity to work in his laboratory and for being my advisor. He has taught me to question everything and seek answers, the first trait defining a researcher. His constant motivations have helped cross many a hurdle. I would also like to thank Dr. Samir Iqbal for giving me access to his lab to perform many experiments. His enthusiasm towards research has encouraged me to never give up easily when presented with a daunting problem.

I would like to acknowledge my friends Waseem Asghar and Mohsin Rizwan for being with me throughout all the highs and lows of research. The many hours spent in discussions and brainstorming have helped me become more innovative and generate solutions to many problems faced in research. I would also like to acknowledge the staff of Nanotechnology Research and Teaching Facility for their patience and assistance with me in the clean room.

I am nothing without my family and I am grateful for their unstinting support and prayers in all of my endeavors.

April 16, 2012

ABSTRACT

DESIGN, MICROFABRICATION AND CHARACTERIZATION
OF A MICROHEATER PLATFORM FOR STUDYING
DNA-SURFACE INTERACTIONS

Annas Javed, M.S

The University of Texas at Arlington, 2012

Supervising Professor: Ankur Jain

The past few decades have witnessed significant research towards developing DNA biosensors and gene chips. These devices obtain sequence-specific DNA information in a faster, simpler and cheaper manner compared to traditional hybridization assays. Miniaturization of DNA handling and processing devices has contributed significantly towards this effort. Despite the large amount of work in this research direction, much more needs to be understood about the physics behind DNA interactions with their microenvironment, particularly with inorganic surfaces. For example, a basic understanding of thermal interactions of DNA with surfaces may help develop novel strategies for probing, purifying and manipulating DNA.

This thesis describes the design, microfabrication and characterization of a microheater device on glass. This device is capable of producing large temperature rise through electrical heating in a thin microheater deposited on the glass substrate. Thermal-electrical design principles behind the design of the microheater device are described. Microfabrication of the device is carried out using photolithography and metal deposition.

Microheaters fabricated on glass slides and glass coverslips are thermally characterized and compared with each other. Experimental data shows a linear dependence of temperature rise on electrical power, which is along expected lines. Data indicates that a temperature rise of over 100 °C may be obtained by passing a relatively small amount of current. Experimental data is found to be in excellent agreement with finite-element simulation results. Simulations are also carried out to understand the transient thermal behavior of the microheater device.

In order to demonstrate the microheater device, experiments are carried out to detach DNA immobilized on the microheater surface through a Streptavidin-Biotin bond. SAM modified glass surface are functionalized with NHS biotin as a linker to streptavidin which can immobilize any biotinylated molecule like biotinylated DNA. It has previously been reported that Biotin-Stretavidin bond can be broken at 70 °C using a non-ionic aqueous solution. Following thermal calibration, DNA is immobilized on the microheater surface, and then experiments are carried out to detach the DNA using the microheater. Fluorescence imaging results show that the fluorescent intensity after heating is considerably lower than before heating, thereby confirming the breaking of Biotin –Streptavidin bond and hence specifically detaching DNA.

The microheater device described in this work may find application in several other areas of bioengineering research. While this work investigated a single microheater line, it would be interesting to study the effect of several strategically placed microheater for producing a desired temperature field. This may aid in DNA analysis chips where controlled attachment, detachment and manipulation of DNA is desirable. Further, the microheater platform may provide a novel thermal interface for studying thermal effects on cells.

TABLE OF CONTENTS

LIST OF ILLUSTRATIONS

Figure Page

LIST OF TABLES

CHAPTER 1

INTRODUCTION

Bio-MEMS stand for biological microelectromechanical systems and it refers to a special class of microelectromechanical systems (MEMS). MEMS being a world of very small devices, when being used to study biological matter, the research area are called Bio-MEMS. The devices and integrated systems using BioMEMS are also called lab-on-a-chip and micro-total analysis systems. Areas of research and applications in BioMEMS range from diagnostics, such as DNA and protein micro-arrays, to novel materials for BioMEMS, micro-fluidics, tissue engineering, surface modification, implantable BioMEMS and systems for drug delivery [1].

Although a lot of MEMS devices have been fabricated and tested in the lab environment, most of these devices are being used for *in vitro* applications [2]. These devices include microreservoirs, micropumps, cantilevers, sensors, and other structures. Research Interest in using MEMS and microfabrication technologies for *in vivo* applications is growing and researchers are trying to develop tools to make use of these devices and implant them in human body. MEMS advantages over other types of implantable systems for certain applications include small size scale, electrical nature, and ability to operate on short time scales.

Bio-MEMS provide a platform for studying the effect of various forces of nature on individual cells and biomolecules. For example, using micro fabricated tools, a known amount of force can be applied on a single cell [3]. Micro fabrication has a special significance in BioMEMS. With the advent of nanotechnology and new fabrication techniques, it is possible to design and manufacture experimental platforms that are of comparable size as typical cells and DNA. These devices are used to detect cells, microorganisms, viruses, proteins, DNA etc., a

sub area of BioMEMS research called bio-sensing. Site specific detection of DNA has been a great focus of research for biologists and chemists in the past two decades to analyze hybridization, PCR amplification and drug delivery [3]. The analysis of complex DNA samples and acquisition of sequence and expression information would require the integration of multiple biosensors in connection with DNA microarrays [4,5]. The use of DNA microarrays is thus revolutionizing many aspects of genetic analysis. The attractive properties of these chips are the miniaturization, accurate measurement and very high speed. Studies have been carried out to study the interactions of these biomolecules with different stimuli like optical tweezers, electrical fields etc. Interaction and immobilization of these biomolecules with different surfaces like glass, silicon and gold etc. have been analyzed. Effect of mechanical, electrical and optical forces on these interactions has been studied but not much attention has been given on thermal effects. The focus of current work is in observing the impact of temperature on these surface interactions. A micro heater device capable of producing a temperature field in a localized area is designed and fabricated.

The thesis explores the use of the microheater device for specifically detaching DNA from inorganic surfaces like glass. Chapter 2 discusses the methods, polymers and different biological molecules that are used in the experiments. Chapter 3 focuses on the design, fabrication and calibration of microheater. In chapter 4, the experiments and results for the DNA experiment are presented. This includes the methods, recipe and equipment used for the experiments and step by step details of the experiment. The results and limitations of the technique are highlighted.

CHAPTER 2

BACKGROUND AND LITERATURE REVIEW

2.1 Microheater Applications in MEMS

The number of applications for MEMS micro-heater devices is increasing rapidly, since microheaters are major components in micro-sensors such as humidity sensors [6] and gas sensors[7]. A MEMS micro-heater that can produce heat by applying an electrical current to a resistor has the advantage of low power driving as well as a very short response time. These days MEMS micro-heaters are becoming very important in portable electronics applications where low-voltage and low-power designs are required. Several investigations have been conducted on micro-heaters that use Silicon Carbide [8], Platinum [6,9-11], poly-Silicon [12], single crystal silicon [13], and Titanium Nitride [14] as the heating element. A study of temperature distribution uniformity over the heating plate through control of the heat distribution was reported [15]. Polyimide [9] and Silicon on Insulator [16] have been studied for use as membrane materials. Silicon micro-heaters have been a subject of intense research within the past decade. Traditionally the interest in silicon microheater devices was largely driven by the need of low power heating elements for gas sensitive metal oxide materials. Moreover, the small thermal inertia of micromachined heater devices allows triggering rapid temperature changes which has opened up new perspectives for developing non-stationary methods of sensor operation [17-20]. As detailed in previous reported literature [21-23] micro heater elements can be realized following two basic architectural designs: (i) closed dielectric membrane and (ii) hotplate devices. The architectural simplicity of the first kind of device is basically enabled by the low heat conductivity of SiO_2 and Si_3N_4, which form the structural membrane materials . In the latter kind of devices, semiconductor materials such as silicon (Si)

or silicon carbide (SiC) are used as structural membrane materials. Due to the much higher thermal conductivities of these latter materials, closed-membrane architectures are no longer possible and hotplate designs need to be introduced to reduce the heat flow from the heated hotplate to the supporting silicon rim. Using this latter approach, relatively sophisticated devices have been realized by co-integrating sensitive materials, bulk Si heaters and electronic read-out chips at the same time [24-25]. Recently, gas-sensitive field-effect devices have been successfully integrated into such devices [26]. Meeting the relatively modest high temperature requirements of such gas-sensing devices platinum (Pt) and polycrystalline silicon (poly- Si) have found wide-spread acceptance as electrically conductive heater materials [27-28]. Building on this work, attempts have been made to introduce novel materials into the micro heater design that allow attaining much higher temperatures in the range of 1300 K or above. Examples are SiC membranes and HfB2 heaters [29]. This has enabled novel applications of micro heater devices become feasible such as thermal IR emitters [30-32], flameless ionization detectors [33] and surface ionization devices [34]. In 2006, work on silicon-on-insulator (SOI) based thermal IR emitters, heated using different heater materials and heater designs. In this work, performance of metal (Pt, PtSi) and semiconductor heater materials (Si:B and SnO2:Sb) were compared and it was concluded that semiconductor heaters provide a significantly better performance at operating temperatures in the 1300 K range

2.2 Device Fabrication

Microheater devices were fabricated in a class 100 cleanroom using lift-off. This section is the literature review of the fabrication process. Below is the detail of all the steps involved in this process.

2.2.1 Photolithography

Photolithography is the process to transfer patterns on a mask to the surface of a substrate such as silicon wafer. The steps involved in the photolithographic process are as follows [35]

1) Wafer cleaning

In order to get a good pattern using lithography, cleaning is the most crucial step. If the wafers are not clean, the pattern may not appear as expected. Typical contaminants that must be removed prior to photoresist coating include dust from scribing or cleaving atmospheric dust, abrasive particles, lint from wipes, photoresist residue from previous photolithography, oil etc.

The well-known process used for cleaning the wafer is called RCA clean and consist of 3 steps. The wafers are first prepared by soaking them in DI water. The first step involves a 1:1:5 solution of NH_4OH (ammonium hydroxide) + H_2O_2 (hydrogen peroxide) + H_2O (water) at 75 -80 °C typically for 10 minutes. This treatment results in the formation of a thin silicon dioxide layer on the silicon surface, along with a certain degree of metallic contamination that shall be removed in subsequent steps followed by transferring the wafers into a DI water bath. The second step is a short immersion in a 1:50 solution of HF + H_2O at 25 °C, in order to remove the thin oxide layer and some fraction of ionic contaminants. The third step is performed with a 1:1:6 solutions of HCl + H_2O_2 + H_2O at 75 or 80 °C.

The surfaces of several commonly used substrates oxidize very quickly. This surface oxide forms hydrogen bonds with water adsorbed from the air which results in poor resist adhesion on spin coating. Hexamethyldisilazane (HMDS) is one of the most commonly used adhesion promoters used to nullify this effect.

2) Photoresist application

Photoresist is a light sensitive material used for photolithography process [35]. There are two types of photoresists

a) Positive Photoresist

In case of positive resists, the resist is exposed with UV light wherever the underlying material is to be removed. The exposure to UV light changes the chemical structure of the resist so that it becomes more soluble in the developer. The exposed resist is then dipped in the

developer solution, leaving windows of the bare underlying material. The mask, therefore, contains an exact copy of the pattern which is to remain on the wafer

b) Negative Photoresist

In case of negative resists, the resist is exposed with UV light wherever the underlying material is not to be removed. The exposure to UV light changes the chemical structure of the resist (cross-linking) resulting in polymerization of resist. The exposed resist is then dipped in the developer solution, removing all the resist except the exposed area. The mask, therefore, contains inverse of the pattern that is there on the mask.

Photoresist is spin coated on the wafer at a specific speed that will determine the thickness of the resist and hence the exposure and develop time.

3) Soft Baking

This step is used to remove any solvent from the photoresist. It is a critical step as excessive baking may affect the photoactive part of the photoresist and reduce sensitivity.

4) Mask alignment

After prebake, the mask is aligned with the wafer to transfer the pattern on the wafer. This is not a critical step for single mask microdevices but is very critical when more than one mask is being used for fabrication.

5) Exposure and Development

Photoresist is exposed to the UV light through the aligned mask. Depending on the tone of resist, the resist will either dissolve or polymerize upon UV exposure. The wafer is then dipped in the developer and agitated well to remove the unwanted photoresist and generate the pattern.

6) Hard-baking

A hard bake or post exposure bake is used to reduce standing waves in regular positive resist exposed on the steppers. Besides that, it also helps to thermally activate chemical processes such as image reversal.

2.3 Metal Deposition Techniques

Two techniques commonly used for making patterns of any evaporated material using lithography are wet etching and lift-Off. Since, the current work utilizes the lift-off method so it is discussed in detail

2.3.1 Lift-Off Method

Lift-off is a simple method for patterning deposited films that are deposited. Figure 2.1 shows the scheme used for the lift off process [36].

A pattern is defined on a substrate using lithography The film of interest is deposited all. After depositing the metal film, the substrate was dipped in a glass beaker filled with acetone and placed in an ultrasonicator. The beaker is left in ultrasonicator for 6-10 minutes to ensure all the resist is dissolved taking off all the metal on top and giving a pattern only on exposed substrate surface.

Depending on the type of lift-off process used, patterns can be defined with extremely high fidelity and for very fine geometries. Lift-off, for example, is the process of choice for patterning e-beam written metal lines. Because film sticks only where photoresist is cleared, the defect modes are opposite to what one might expect for etching films.

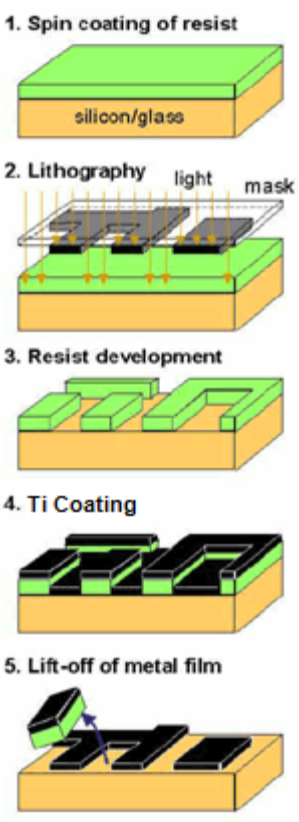

Figure 2.1: Lift-Off Process Schematic [36]

There are some constraints on the process as well. Any deposited film can be lifted-off, provided. The foremost constraint in lift-off is that during film deposition, the substrate does not reach temperatures high enough to burn the photoresist [37].In addition other constraints include the film quality is not absolutely critical and photoresist will outgas very slightly in vacuum systems, which may adversely affect the quality of the deposited film. Also, adhesion of the deposited film on the substrate is very good; the film can be easily wetted by the solvent. The film is thin enough and/or grainy enough to allow solvent to seep underneath. The film is not elastic and is thin and/or brittle enough to tear along adhesion lines

2.4 DNA immobilization techniques

It is important to properly immobilize the DNA on glass surface. Unfortunately, typical insulators do not have a high tendency to form bonds with the termination of a DNA strand [38]. There are many different methods that allow DNA strands to be immobilized [39].

a. **Physical or chemical adsorption**. This is generally done between the insulator and the bases of the probe. This will cause weak immobilization and will also make the hybridization of targets harder, due to the limited mobility of the probe.
b. **Cross-linking**. This method utilizes materials with inner structure, such as nanoparticles or polymer matrix assemblies. Such materials can help sustain the DNA in a position close to the surface of the insulator.
c. **Covalent attachment**. This method relies on functionalizing the surface of the insulator with a self-assembled monolayer (SAM). The SAM is used to covalently bond to the gate insulator at one end, and to the DNA probe at the other end. An example of a material used to bind DNA probes to SiO2 surface is APTES (3-aminopropyltriethoxysilane) [40].
d. **Entrapment**. The DNA molecules can be entrapped inside a gel matrix or paste, keeping it close to the sensitive surface

Although one might expect that a higher probe density will result in a higher amount of hybridized charge and better sensitivity, it has been shown [41] that higher probe densities result in reduced hybridization efficiencies as can be seen in Figure 2.2

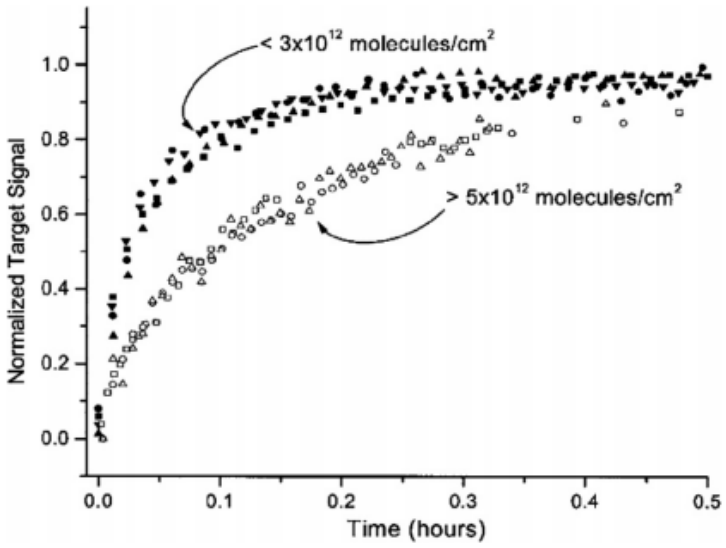

Figure 2.2: Hybridization efficiency curves for different DNA probe densities [42]

Keeping in mind all these factors, a recipe for a specific concentration of Streptavidin was adopted. Since this work involves temperature driven breaking of Streptavidin-Biotin bond, covalent attachment technique was preferred and utilized. Although the physical or chemical adsorption immobilization techniques are simple but they result in weak immobilization.

2.5 Surface Chemistry Background

This section discusses the details of all the chemicals and biomolecules used and their significance in the current experiment will be discussed.

2.5.1 Self-Assembled Monolayers

SAMs are ordered molecular assemblies formed by the adsorption of an active surfactant on a solid surface as shown in Figure 2.3. SAMs, are formed when surfactant molecules spontaneously adsorb in a monomolecular layer on surfaces. A SAM is utilized various applications, such as protein immobilization [43-44], mineralization or surface modification by utilizing two different functional groups, at each end of the SAM molecule. SAMs offer a unique combination of physical properties that allow fundamental studies of

interfacial chemistry, solvent-molecule interactions and self-organization. Their well-ordered arrays and ease of functionalization make them ideal model systems in many fields [45].

The field of self-assembled monolayers (SAMs) has witnessed tremendous growth in synthetic sophistication and depth of characterization over the past few decades [46]. However, it is interesting to comment on the modest beginning and on important milestones. The field really began much earlier than is now recognized. In 1946 Bigelow *et al* published the preparation of a monomolecular layer by adsorption (self-assembly) of a surfactant onto a clean metal surface [47].

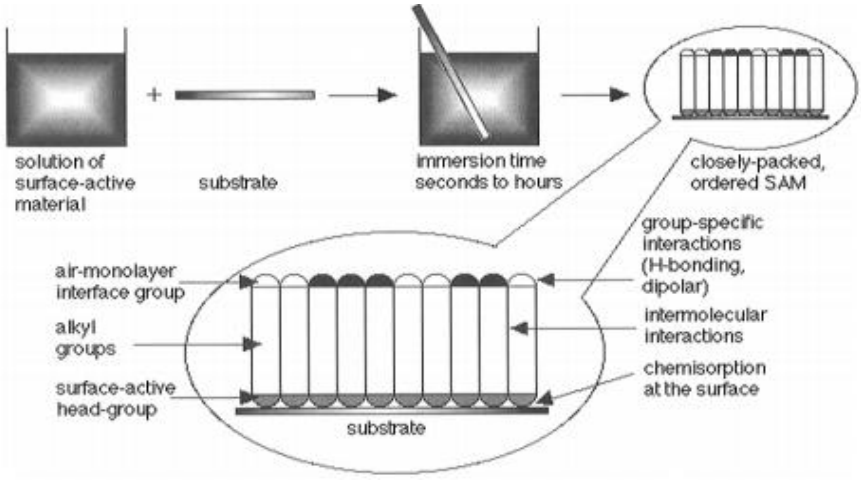

Figure 2.3: Self-assembled monolayers are formed by simply immersing a substrate into a solution of the surface-activematerial. The driving force for the spontaneous formation of the 2Dassembly includes chemical bond formation of molecules with the surface and intermolecular interactions[46]

This simple process behind developing SAMs on substrates makes them inherently manufacturable and thus technologically attractive for building super lattices and for surface engineering. The order in these two-dimensional systems is produced by a spontaneous chemical synthesis at the interface, as the system approaches equilibrium. Although the area is not limited to long chain molecules, SAMs of functionalized long-chain hydrocarbons are most frequently used as building blocks of super molecular structures [48]

2.5.2 Types of SAMs

The application of the Self assembled monolayers decides the selection of specific type of head group [49]. In most cases, head groups are connected to an alkyl chain in which the terminal end can be functionalized to vary the wetting and interfacial properties.[50-51]. An appropriate substrate is chosen to react with the head group. Substrates can be planar surfaces, such as silicon and metals, or curved surfaces, such as nanoparticles. The most commonly used molecules for SAMs are alkanethiols. These are the molecules with an alkyl chain, $(C\text{-}C)^n$ chain, as the back bone, a tail group, and a S-H head group. They are used on noble metal substrates because of the strong affinity of sulfur for these metals. The sulfur gold interaction is semi-covalent and has strength of approximately 45kcal/mol. Gold is an inert and biocompatible material that is easily available. It is also easy to pattern via lithography[49] and can withstand harsh chemical treatments [52] Silanes are generally used on nonmetallic oxide surfaces [49] however monolayers formed from covalent bonds between silicon and carbon or oxygen cannot be considered self-assembled as they do not form reversibly. A special case are SAMs of thiolates on noble metals since the metal-metal bonds become reversible after the formation of the thiolate-metal complex.[53] This reversibility is something that gives rise to vacancy islands and that is why SAMs of alkanethiolates can be thermally desorbed and undergo exchange with free thiols.[54]. In our experiment, 3-APTES will be used which generates -NH2 as a functional group on glass surface which attracts the NHS biotin, the cross linker between SAM and streptavidin.

2.6 Streptavidin-Biotin Interaction

2.6.1 Biotin

The streptavidin biotin bonding provides an effective method to characterize, separate and detect other biological molecules [55]. Biotin also known as Vitamin H is a water soluble B-complex vitamin. Biotin is used for preventing and treating biotin deficiency associated with

pregnancy, long-term tube feeding, malnutrition, and rapid weight loss [56]. It is also used orally for hair loss, brittle nails, skin rash in infants, diabetes and mild depression. The chemical structure of biotin is shown in Figure 2.4.

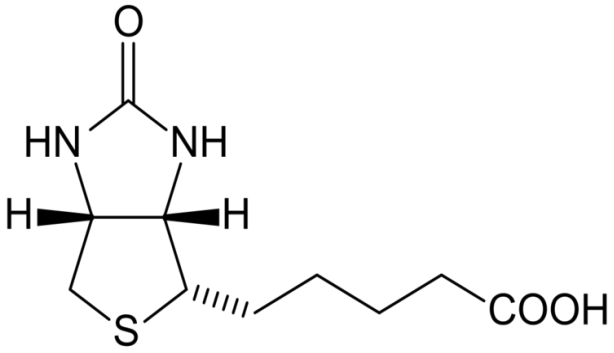

Figure 2.4: Chemical Structure of Biotin [56]

2.6.2 Streptavidin

Streptavidin is a tetrameric protein that binds strongly to biotin [57]. This high affinity of the noncovalent interaction between biotin and streptavidin forms the basis for many diagnostic assays that require the formation of an irreversible and specific linkage between biological macromolecules. The binding of biotin to streptavidin is one of the strongest non-covalent interactions known in nature. The dissociation contant of this bond is on the order of $\approx 10^{-14}$ mol/L. [58]. When the refined crystal structures of apo and a streptavidin-biotin complex was compared, it showed that the high affinity results from many factors. These factors include the formation of multiple hydrogen bonds and van der Waals interactions between biotin and the protein, together with the ordering of surface polypeptide loops that bury the biotin in the protein interior [57]. Structural alterations at the biotin binding site produce quaternary changes in the streptavidin tetramer. These changes apparently propagate through cooperative deformations in the twisted beta sheets that link tetramer subunits. Figure 2.5 shows the tetrameric structure of Streptavidin.

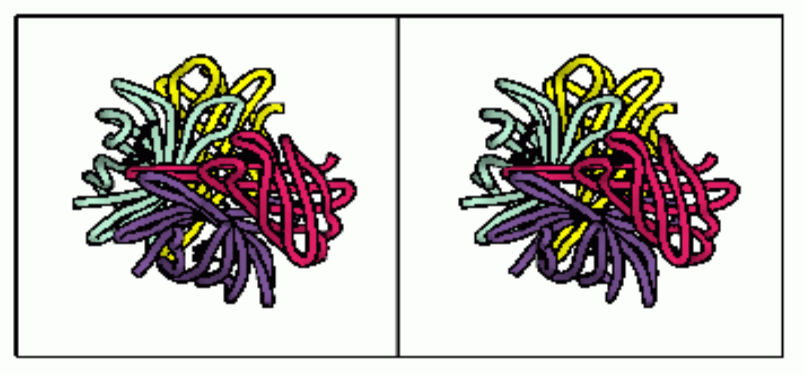

Figure 2.5: Tetrameric Structure of Streptavidin [59]

Avidin, streptavidin or NeutrAvidin Protein can bind up to four biotin molecules, which are normally conjugated to an enzyme, antibody or target protein to form a streptavidin-biotin complex. Streptavidin's lack of glycosylation and lower pI results in a lower degree of nonspecific binding, especially lectin binding, compared to that observed for avidin in immunohistochemistry applications. This makes streptavidin an ideal reagent choice for many detections systems. Figure 2.3 shows a schematic illustration of this bond formation.

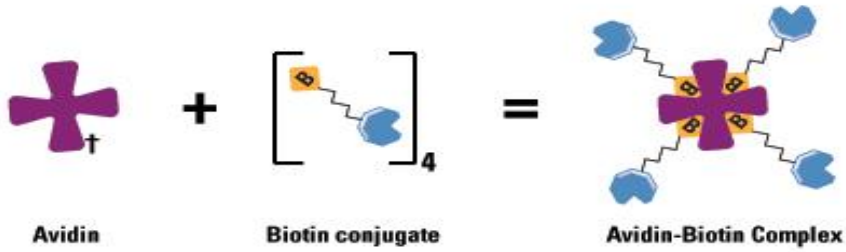

Figure 2.6: Biotin-Avidin Bonding Schematic [60]

The streptavidin-biotin interaction can be used for detecting a diverse number of targets with three different basic configurations (61-63): (a) where streptavidin is labeled with a detectable molecule, e.g., an enzyme, fluorescent, chemiluminescent, or radioactive probe or some other moiety. Biotin present in another reactant such as anantibody, nudeotide, Protein A, lectin, etc, links the target molecule with the labeling system. This detection format is used

widely for immunoassays, DNA hybridization assays, immunohistochemistry, and flow-cytometry. Avidin and streptavidin conjugates carrying a variety of detectable molecules are commercially available (b) Streptavidin is used unlabeled and serves to link the biotinylated binder with the biotinylated detection molecule. This variation of the system takes advantage of the multiple biotin-binding sites in each avidin or streptavidin molecule. It is also used widely in immunoassay and DNA hybridization techniques, especially with probes that can be easily biotinylated such as enzymes etc.

2.7 Biotinylation

Biotinylation is the term used in biochemistry to covalently attach DNA, RNA, proteins and other biomolecules to biotin. The biotinylation process is very useful in observing the properties like hybridization, specific attachment and protein purification. In our work, biotinylated DNA's were used in our functionalization technique to immobilize DNA on streptavidin coated glass surface. One of the basic components in a biotin-streptavidin based system is the biotinylated moiety, which can be a protein, a polysaccharide, a nucleic acid, a low-Me substance, etc. To biotinylate such diverse classes of compounds, researchers have developed several different biotinylation reagents (active biotin derivatives). In addition, other biotinylation reagents have been developed for specific applications: e.g., cleavable reagents that can be used for biotinylation with the option of removing biotin at a later stage by reduction of a disulfide bond or hydrolysis of phenyl ester linkage [64-67].

2.7.1 Biotinylation of DNA

Nucleic acid biotinylation can be accomplished with several different procedures, most ofwhich have evolved very recently. In general, cloned nucleotide fragments are biotinylated with different strategies from those used with small synthetic oligonucleotides. The major interest in biotinylating nucleotides arises mainly from the need to devise highly sensitive nonisotopic hybridization assays. Many procedures for nucleic acid biotinylation are based on

enzymatic catalysis; others are chemical methods. Enzymatic biotinylation procedures rely on the availability of biotinylated nucleotide analogs that can act as enzyme substrates. Alternatively, nonbiotinylated nucleotide derivatives can be used as substrates but, after they are incorporated into DNA, they can be chemically biotinylated because they carry into their structure an easily biotinylable group.

The first reported biotinylated nucleotides were biotinylated uridine triphosphate (UTP) and deoxyuridine triphosphate (dUTP)[68-69]. Another useful class of biotinylated nucleotides consists of nucleotides that contain the S-S group within the structure of the linker arm. These “releasable” nucleotide analogs can be used in applications where the nucleic acid needs to be released after its binding to streptavidin [70-71].

CHAPTER 3

DESIGN AND FABRICATION

This chapter analyzes the microheater device fabrication and the key parameters considered to design the device. The detailed procedure followed to fabricate the device will be discussed. A brief overview of the equipment use in the cleanroom will be given. After that, the calibration procedure on the device and results will be discussed. In the last section simulation results will be presented and compared with the experimental data.

3.1 Design Considerations

In this subsection all the necessary design considerations before fabricating the device will be highlighted.

3.2 Selection of Wafer

For the fabricaton of microheater devices, a substrate with a low thermal conductivity should be slected. Heat transfer across materials of high thermal conductivity occurs at a higher rate than across materials of low thermal conductivity. For this experiment a specific temperature in the area close to the heater is desirable and the heat should not diffuse away due to thermal conduction. At room temperature, the thermal conductivity of glass and silicon are 0.8 $W \bullet m^{-1} \bullet K^{-1}$ [72] and 149 $W \bullet m^{-1} \bullet K^{-1}$ [73] respectively. For that reason, glass was selected instead of silicon wafer since it has a much lower thermal conductivity compared to silicon and is a poor conductor of heat. Table 3.1 shows the thermal conductivities of different elements.

For our experiment, the target temperature is in the range of 70-90 °C. Since, the thermal conductivity is also a function of temperature; the need is to make sure that the thermal conductivity is still in limits during the experiment. Figure 3.1 shows this effect.

Table 3.1: Thermal Conductivities of common engineering Materials [74]

Material	Thermal conductivity
	(W/m K)*
Diamond	1000
Silver	406
Copper	385
Aluminum	205
Iron	79.5
Steel	50.2
Lead	34.7
Mercury	8.3
Ice	1.6
Glass,ordinary	0.8
Silicon	149
Wood	0.12-0.04
Air at 0°C	0.024

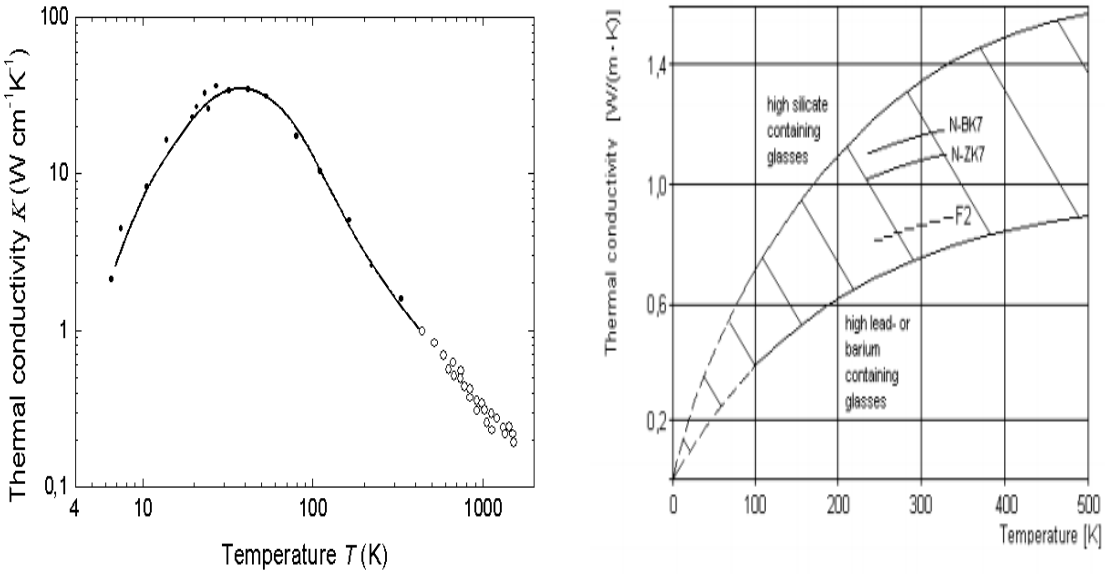

(a) (b)

Figure 3.1: a) Temperature dependence of Thermal Conductivity of Glass [74] b) Temperature dependence of Thermal Conductivity of Glass [75]

As can be seen clearly that the thermal conductivity of Silicon at 70 °C is much higher than glass. So, glass is the choice of material for wafer in our experiment.

3.3 Selection of Metal

While gold is the most widely used metal in bioelectronics, Nickel and Titanium are the most widely used metals for microheater applications. Both of these metals have very high electrical resistivity and high resistance to corrosion. The resistance is directly proportional to resistivity, so higher resistivity corresponds to higher resistance implying more power dissipation and hence more heat generation by passing the same amount of current. Table 3.2 provides a list of some of the metals and their electrical resistivity at 20 °C.

Since a lot of biochemicals and fluids have to be used to functionalize the area near the microheater, so the metal should not corrode. As a result metals like aluminum and iron are not a good choice for us. Another concern is to pass a low current through these microheater devices to avoid breaking of device due to electromigration. Electromigration refers to a commonly encountered break-down phenomenon in metal lines where application of high current density results into a break in the continuity of the metal line. When electric field is applied on the metal strip, the electrons in the metal move under the influence of the large current density [76]. If a charged defect in the metal is encountered, the momentum transfers from the conduction electrons to that defect. In due course of time, the momentum exchange becomes large leading to the build-up of a force causing the atoms to move away from the defect. This results in the breakdown of the metal at that point. Added to this, the heating of the wire speeds up this process of breaking. Both the heating and the momentum exchange increase with an increase in the current density in relation with the applied electric field or the applied voltage. Usually, in these experiments, a threshold current is observed. This indicates the existence of an energy threshold required to induce the electromigration of metal atoms.

While designing devices at micro to nano scales, electromigration plays a key role in determining the dimension of the device.

Table 3.2: Electrical Resistivity of Common materials

Element	Resistivity at 20 °C (Ω.m)
Aluminum	2.82 x 10-8
Carbon (Graphite)	3.5 x 10-5
Constantan	4.9 x 10-7
Copper	1.7 x 10-8
Germanium	4.6 x 10-1
Glass	1010 to 1014
Gold	2.44 x 10-8
Iron	1.0 x 10-7
Lead	2.2 x 10-7
Manganin	4.82 x 10-7
Mercury	9.8 x 10-7
Platinum	1.1 x 10-7
Quartz (fused)	7.5 x 1017
Silicon	6.40 x 102
Silver	1.59 x 10-8
Titanium	4.2 x 10-11

The goal of selecting a metal for this experiment was to avoid a large current which can result in electromigration. Since all the heating through a metal occurs due to Joule heating given by, $P=I^2R$, where current is limited by electro migration. Simulations results showed that

temperature rise is directly proportional to power which in turn is directly proportional to current and resistance. The relationship between resistance and resistivity is given by the following formula.

$$R = \rho L/A \qquad (3.1)$$

where ρ is the electrical resistivity of the material, L is the length of the heater line and A is the area calculated by multiplying width and thickness of the metal line. As resistance is directly proportional to electrical resistivity, material with higher resistivity would be better suited for our application. A very small current should be able to produce large temperature resulting from power dissipation. Also, since this device will be used as a temperature sensor; i.e when there is a change of resistance observed it can be determined that how much heat was being generated that resulted into this change. To measure this resistance change, voltage across the metal line needs to be measures. Keithley instruments were used to observe this voltage change. ΔR/ΔT is very critical in this case since the sensitivity of the instruments should be considered as well. For all these reasons Titanium was selected, since it has a very high electrical resistivity (Table 2.1), provides expected temperature rise at a lower current and gives measurable value of ΔR/ΔT with the dimensions specified below.

Length =25 mm, Width = 20um and thickness 200 nm. Resistance was measured using Eq. 3.1.Since the electrical resistivity (ρ) of Titanium is 420 nΩ·m, the theoretical base resistance *R* can be calculated to be 2625 Ω at room temperature.

3.4 Temperature Vs Resistance

It is very crucial to discuss about the resistance dependence on temperature at this point. The electrical resistance of a conductor such as Titanium is dependent upon collision between charge carriers and the lattice. As the temperature increases, the resistance could be expected to increase with temperature since there will be more collisions. The change in resistance as a function of temperature is given by the following formula.

$$\Delta R = \alpha R \Delta T \qquad (3.2)$$

So, the change in resistance is directly proportional to change in temperature. α for Ti is 0.0038 $°C^{-1}$. With this value and R calculated above, ΔR/ ΔT is calculated to be 9.93 Ω /°C. This shows that the Titanium heater can be used as a temperature sensor as well. The minimum current used to measure the resistance is 10uA, which corresponds to following change in voltage.

ΔV= 10uA* 9.93 Ω /°C

= 993 uV for 1°C

This means that for 1°C change in temperature, the instruments sensitivity should be higher than 993 uV. Since Keithley 2612A source meter is able to sense a voltage change 1uV so this design works perfectly fine for us.

In the later sections of this chapter the experimental and simulation results will be discussed. Graphs showing resistance dependence on temperature and current will be presented to confirm the theoretical and experimental data. A linear curve between temperature change and resistance change is expected.

3.5 Materials and Methods:

The mask was prepared using AutoCAD with the dimensions mentioned above. Figure 3.2 shows the image from AutoCAD.

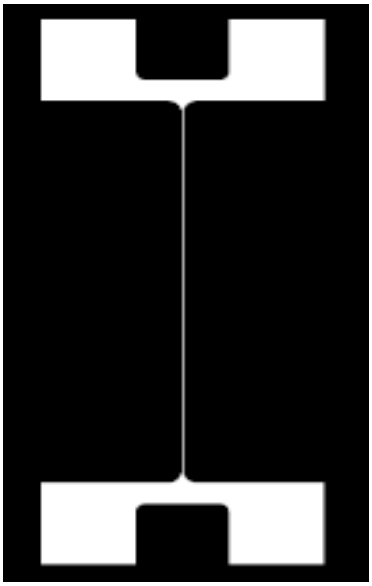

Figure 3.2: Mask Image from AutoCAD

Using this mask for photolithography, lift-off was used to deposit Titanium on the glass slide.

3.5.1 Chemicals

The major chemicals used for fabrication of device include Shipley S1813, MF-319 developer and HMDS

3.5.2 Recipe Used

Below are the steps followed to fabricate the device.

1) Glass slides were cleaned using Piranha solution (1 H2O2: 3 H2SO4), followed by wash with DI water and blow dry under nitrogen
2) Bake the slide at 90 C for 5 minutes to remove any moisture from the surface and then let it cool down
3) Photoresist (S1813) was spin coated at 4000 rpm for 30 sec.
4) PreBake- Coated glass slides were baked at 105 C for 1 minute
5) After prebake slides were exposed to UV light for 15-18 seconds using KarlSuss-MA56 Aligner.

6) Develop for 20 seconds and check the pattern under the microscope
7) Bake at 40 C for 3 minutes to remove all the moisture
8) 200 nm thick Ti was deposited on the patterned slides at a rate of 1 Angstrom/sec using AJA ebeam evaporator. A slower deposition rate makes sure that metal adheres well on the glass surface
9) Ultra sonication in Acetone for 6 minutes removed all the resist giving the desired pattern of titanium.

Figure 3.3 shows the image of the microheater device wired up with copper wires using conductive epoxy.

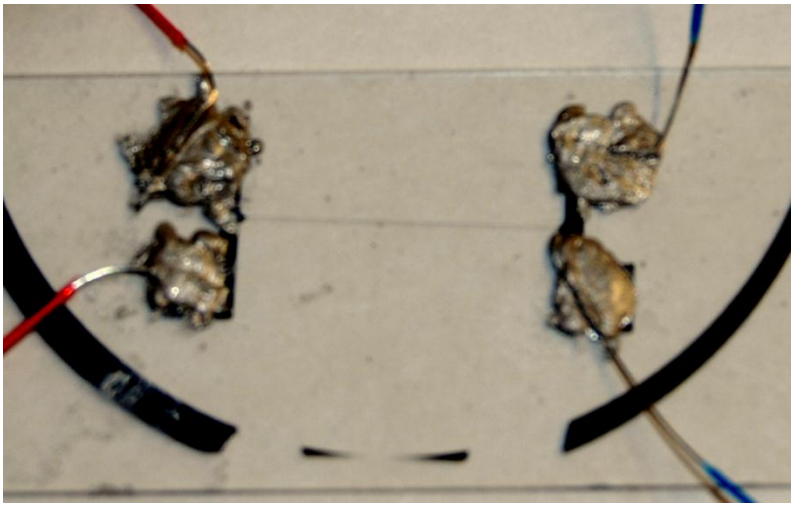

Figure 3.3: Microheater Device after Fabrication

3.6 Micro heater Simulation in ANSYS

Thermal modeling of microsystems was done using ANSYS, a finite element computational software. The overall procedure is to define the geometry, mesh it, provide heat flux and other boundary conditions and then run the simulation to determine the temperature profile. In the following sections, step-by-step details of the simulation steps will be discussed.

First a geometry of the glass slide was defined in ANSYS with a metal line and was meshed. The area close to heater line was meshed particularly fine since this is the area where most of the heat will be concentrated and the most accurate value in this area is desirable. Heat loss from glass slide to the ambient is modeled using a convective heat transfer coefficient and a value of 50 W/m^2 K is specified. This value is typical for natural convection where no forced air flow is provided. Three types of simulations were carried out.

3.6.1 Grid Independence

The simulation geometry was meshed. The number of elements in the mesh directly affects the quality of the results. In order to obtain accurate temperature results, the number of elements in the mesh structure is very critical. There is a certain number of elements range beyond which the temperature field is independent of the element current. This is the threshold value of the number of nodes/elements. This is the least t number of elements that should be used to get the right value of temperature rise. In our simulation, in order to determine the optimum number of nodes, six cases with different number of node elements ranging from 35000 to 1 million were tried. Figure 3.4 shows the mesh structure for the cases of 35 K and 426K elements. In case (b), the mesh is very dense compared to case (a). Keeping the node numbers beyond the threshold value will take extra time in simulation. Keeping the number lower might not give the right value of temperature rise.

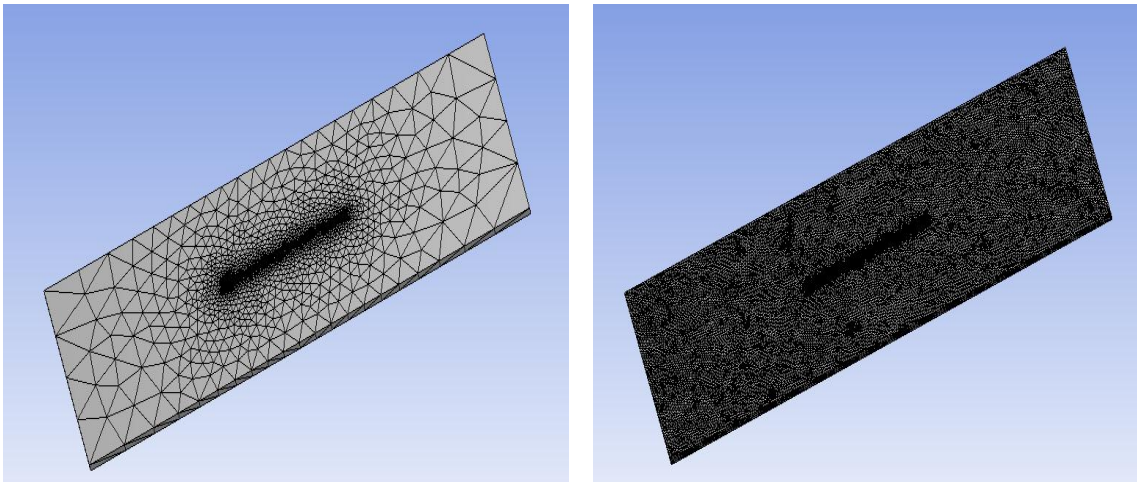

(a) (b)

Figure 3.4: Mesh structure for a) 35K elements b) 426K elements

A plot between number of nodes and temperature rise shown in Fig 3.5 shows the minimum number of elements needed for the simulation to give the right value of temperature rise.

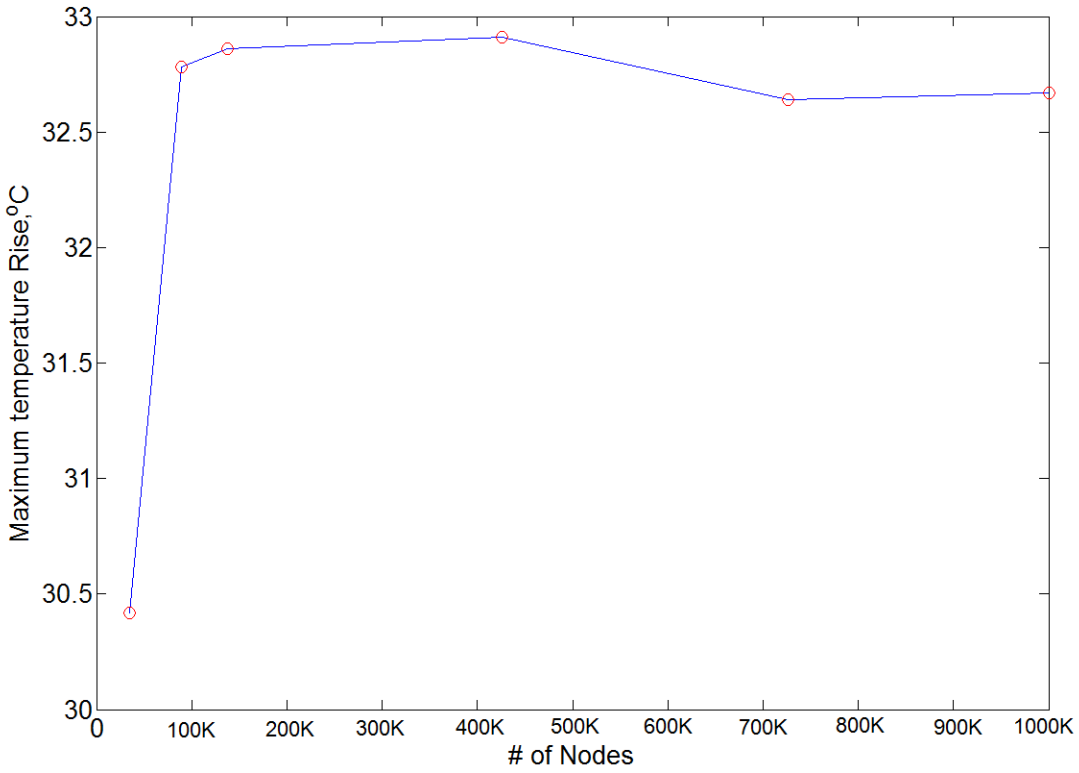

Figure 3.5: Plot between Maximum T_{rise} and Number of Nodes

As can be seen from Figure 3.5, the temperature rise value stabilizes after almost 125 K number of nodes. This is the minimum number of node elements that should be used in the rest of our simulation. 138 K value was selected to be the optimum value for our rest of the simulation.

3.6.2 Transient Simulation

Due to the non –zero thermal mass of the glass substrate it takes time for the thermal field to set up once current starts flowing. To analyze the time required for the device to heat up to the final value, a transient simulation was run. Multiple transient times were tried each with a step of 0.01 seconds. The temperature rise at different times was calculated. Figure 3.6 shows the contour plots of thermal field with time. At t=0 there was no heat and hence no temperature rise. As time passes, the generated field will diffuse through the glass slide.

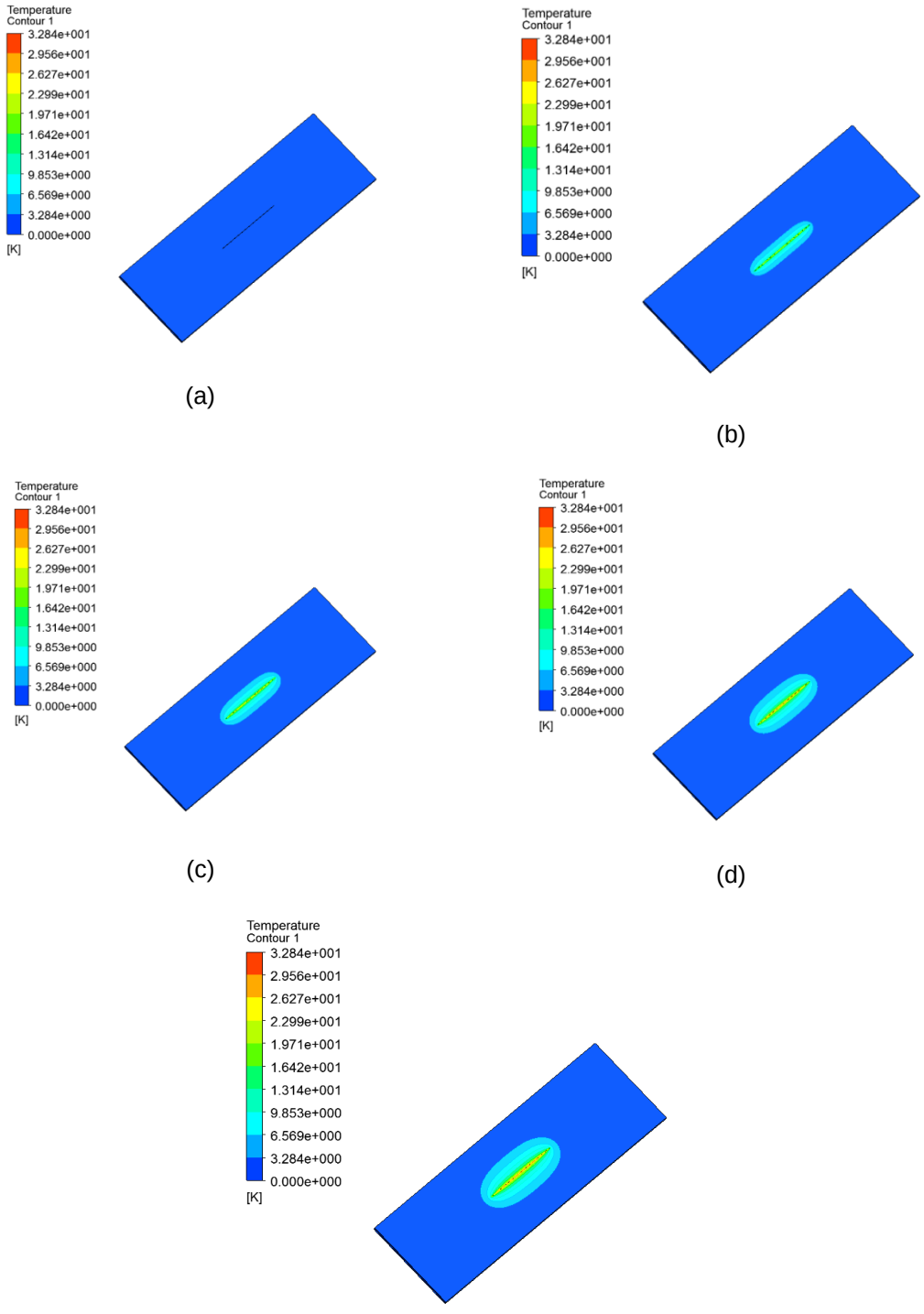

Figure 3.6: Thermal Field at (a) t= 0 sec (b) 7.5 sec (c) 12.5 sec (d) 22.5 sec (e) 35 sec

The temperature rise value at different times was determined through a transient simulation. Figure 3.7 shows that it takes almost 30 seconds for the field to completely set up and reach the final value of 32°C for the specific power used in this simulation.

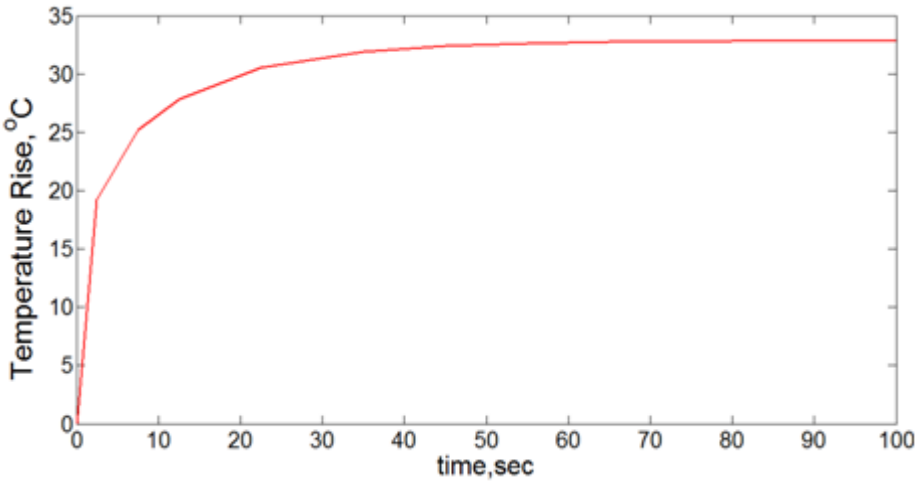

Figure 3.7: Transient Simulation showing temperature field dependence on time

As can be seen from the contour plots, the thermal field diffuses through the glass slide with time and the regions away from the heater line also gets hotter and hotter with time. Figure 3.8 shows the temperature rise value relative to distance, x from the heater line. Note, that the maximum temperature at the heater line, and at a specific point away from the heater line keeps on increasing. The T value stabilized to its final value (32°C) after a certain time (30 seconds approximately) which can be seen from the T value at x=0. If the goal is to set temperature field to setup faster, a coverslip as a substrate can be used instead of glass slide due to lower thermal mass of the coverslip.

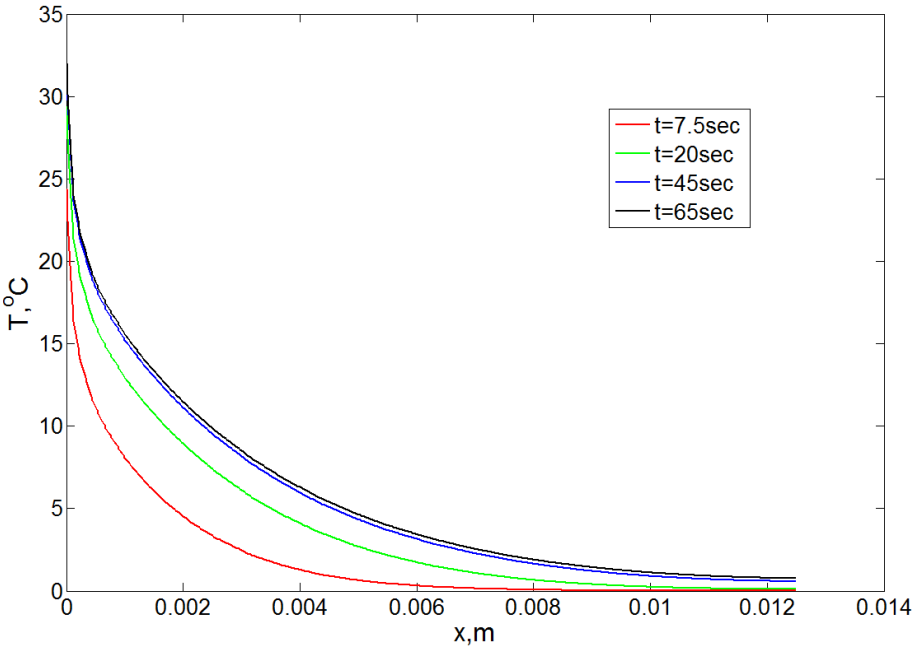

Figure 3.8: Temperature variations along the surface

The plots in Figure 3.8 show the space dependent temperature field, i.e a thermally affected region close to the heater and an unaffected region far from it..

3.6.3 Current vs. Temperature Rise Simulation

In order to simulate the temperature change dependence on current, six different cases of varying currents were tried and the value of temperature rise was recorded. The six currents used 0.6mA, 1 mA, 3mA, 5 mA, 7 mA and 9 mA. Power was calculated using $P= I^2R$, where R is the corresponding resistance value obtained from the calibration data. For each case heat flux was calculated using Q=P/A and the variable was set in ANSYS.Temperature rise values from each simulation was recorded. Figure 3.9 shows the temperature rise as a function of the electronic power. As expected, the temperature rise is linearly proportional to P.

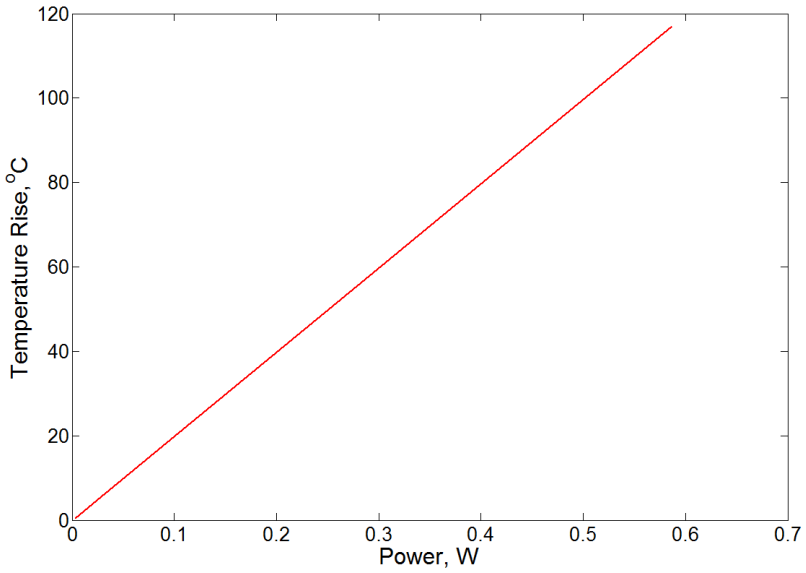

Figure 3.9: Temperature Rise Dependence on Power

3.7 Calibration

The goal of this calibration process is to determine a relationship between temperature and electrical resistance of the heater. This helps in determining the temperature field through an electrical measurement.

3.7.1 Calibration Setup

After making the tight connections of copper wire with the contact pads, the device was placed on the thermal stage by Instech (Instec HCS622). This stage has a temperature resolution of 0.1 °C and is designed for applications where temperature and atmospheric control are critical. The inner connections of the device with the stage were made and the lid of the Instec equipment was closed to avoid any effect of atmospheric conditions during calculations.

Keithley 2612 A source meter from Keithley was used to connect the probes (which are in direct connection with the wires coming from the device contact pads) of the Instec equipment. The setup is ready for experiments and is shown in Figure 3.10.

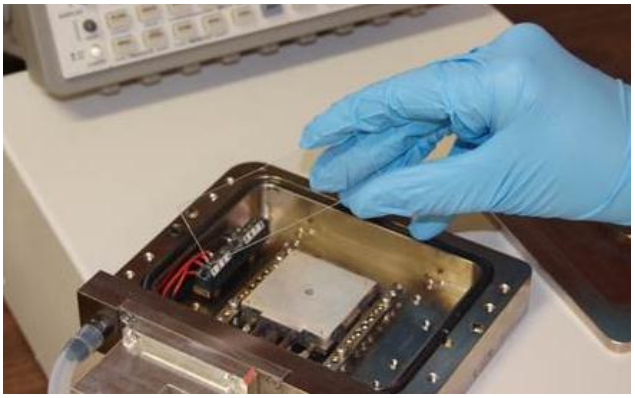

(a)

(b)

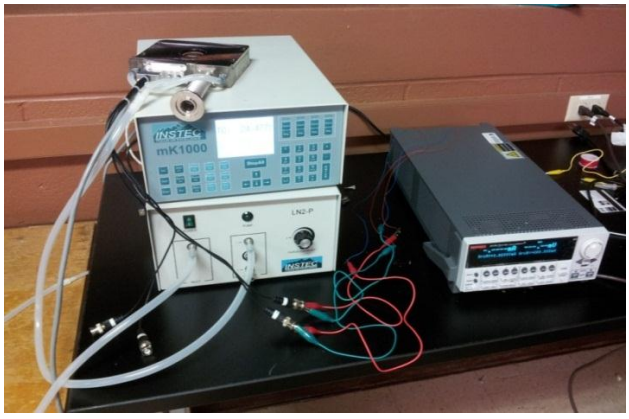

(c)

Figure 3.10: (a) Microheater device with thermal stage (b) Device with wired connections to the stage (c) Connections of thermal heater to Keithley 2612A source meter

As it can be seen from Figure 3.3, the device has 4 contact pads attached to a micro heater line. Two of the contact pads separated by micro heater were used to source the current and the other two were used for measuring the voltage

3.7.2 Calibration Procedure

The calibration procedure can be divided into two steps.

Step 1:-

In the first step, a constant current was applied through the device and kept on changing the temperature to see the effect on resistance. A test current of 10 uA was used since this low value ensures negligible self-heating. The experimental base resistance (R') was calculated. Voltage change with temperature was measured and corresponding resistances were calculated using Ohm's law. Change in resistance with temperature was observed and ΔR/ ΔT was calculated. Table 3.5.1 shows the observed response.

Table 3.3: Resistance dependence on temperature

	T (°C)	R(ohm)
I=10uA	23	3281
	26	3310
	30	3350
	35	3401
	40	3450
	45	3502
	50	3550
	55	3598
	60	3648
	65	3696
	70	3745
	75	3794
	80	3847
	85	3898
	90	3956

The observed base resistance value was 3281 ohms which is close to calculated value of 2625 Ω. The higher value might be a result of many possible reasons. First, the electrical resistivity of thin films is usually higher than bulk material. Also, there may be variations in line width since photolithography may shrink the metal line if underexposed. Further, the metal deposition process may not have deposited the targeted metal thickness. As can be seen from the table, the $\Delta R/\Delta T$ = 10.3 Ω/°C. This means that with every 1°C rise in temperature the resistance increases by 10.3 Ω. This forms the basis of our second step.

Step 2:-

In the second step, a range of currents 0.1mA-9mA was passed through the device while the ambient was maintained at a constant temperature. The corresponding voltages for each case were measured and resistances were calculated. The resistance value changes at higher currents because of heat generated due to power dissipation through the device, since power dissipation can be given by

$$P=I^2R \qquad (3.4)$$

Based on the change in resistance, the temperature rise was calculated since $\Delta T = \Delta R/10.3°C$. Table 3.5.2 shows all the calculations.

Table 3.4: Temperature dependence on Current

I (mA)	V (V)	Rm(Ω)	ΔR =Rm-R'(Ω)	ΔT =ΔR/10(°C)
0.1	0.3289	3281	0	0
0.2	0.657	3281	0	0
0.6	1.972	3281	0	0
0.9	2.96	3284	3	0.3
1	3.289	3289	7	0.7
2	6.599	3299.5	18	1.8
3	9.952	3317.3	36.3	3.63
5	16.881	3376.2	95.2	9.52
6	20.51	3418.3	137.3	13.73
7	24.3	3471.4	190.4	19.04
9	32.6	3622.2	341.2	34.12

As can be seen from the table, a noticeable change in resistance was observed at higher currents. This is because at lower currents, the power dissipation is not enough to contribute to resistance change. Using the values in table the temperature generated is determined at a specified current. For example, in order to generate a temperature rise of 19 °C, 7mA of current should be passed through the device. Note, that this is only the temperature rise. In order to calculate the total temperature close to heater line, the room temperature should be added.

$$\text{Temperature} = \Delta T + T_{room}\ ^{\circ}C \qquad (3.5)$$

Plots between R vs T and Poer vs Temperature Rise were drawn and are shown in Fig 3.11.

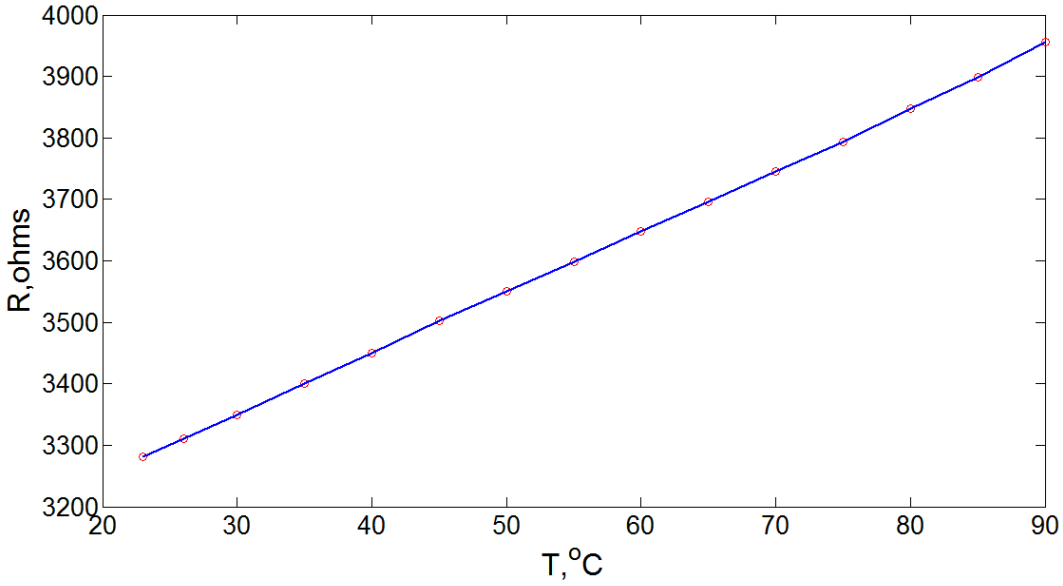

(a)

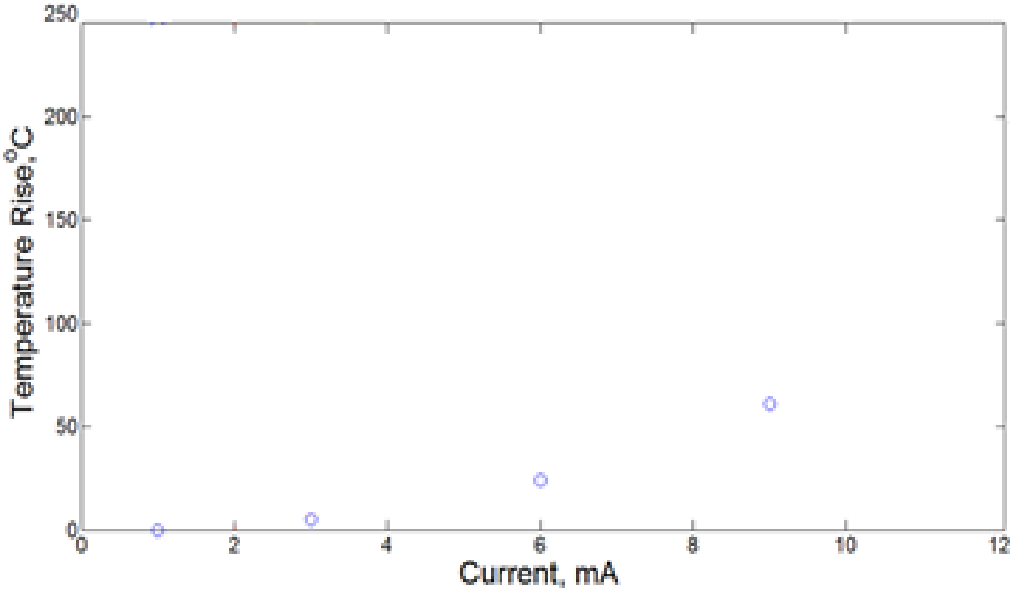

(b)

Figure 3.11: Graph for a) Step 1 of Calibration showing T vs R relationship b) Step 2 of Calibration showing I vs Temperature Rise plot

Note that resistance is linearly proportional to temperature while temperature has a square relationship with current as expected.

3.7.3 Comparison with Simulation Results

Figure 3.12 compares the experimental data with simulation results. It can be seen that experimental data is in excellent agreement with simulation results.

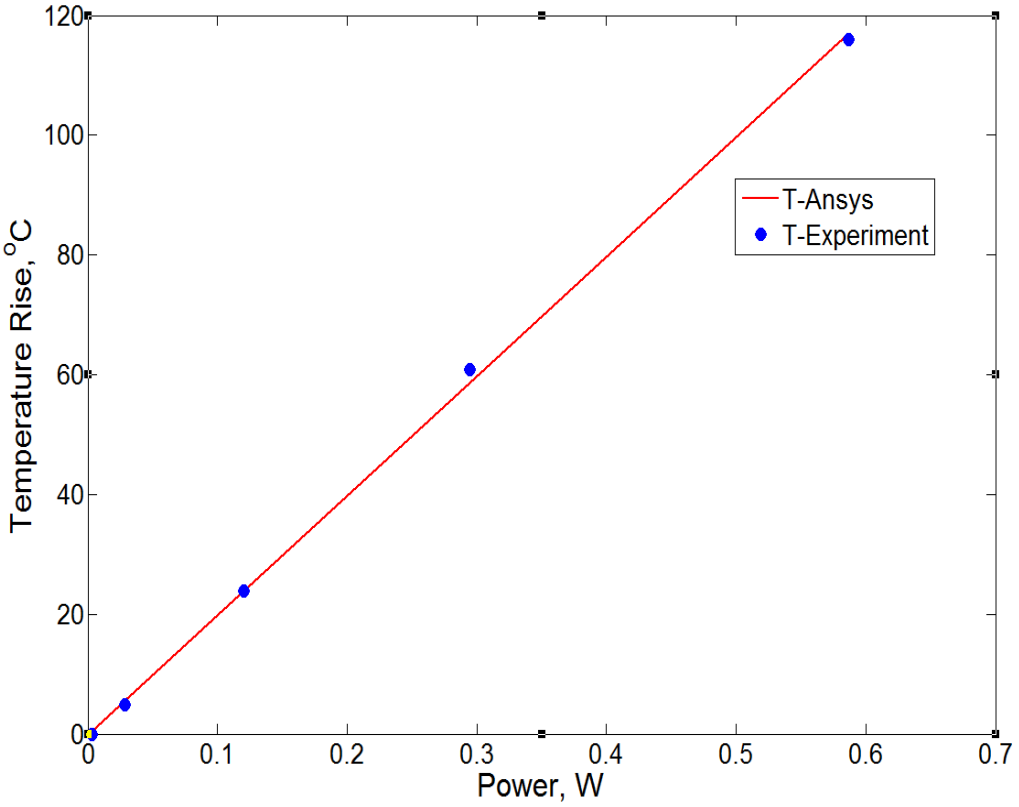

Figure 3.12: Comparison between Simulation vs Experimental Data

3.7.4 Comparison of thermal performance of a Glass Slide and a Cover Slip

The temperature rise is also dependent on the thermal mass of the substrate. The specific heat capacity is defined as the amount of heat per unit mass required to raise the temperature by 1 °C and given by the following formula

$$c = Q/m\Delta T \qquad (3.4)$$

where Q is the heat added, 'ΔT' is the temperature rise, 'm' is the mass and 'c' is the specific heat. In order to determine the right substrate thickness to generate the required temperature, micro heater device was fabricated both on the coverslip and glass slide.

Table 3.5: Resistance change of Microheater with current on a cover slip

I-cover (mA)	V-cover (V)	Temperature Rise (^{o}C)
1	2.754	0
2	5.555	3
3	8.469	11
4	11.55	21
8	27.01	75
12	53.6	225

. Tables 3.5 and 3.6 show the data recorded for both the coverslip and glass slide in the cleanroom using the probe station.

Table 3.6: Resistance Change of Microheater with current on a glass slide

I-slide(mA)	V-slide (V)	Temperature Rise (^{o}C)
1	3.147	0
3	9.56	8
6	20.03	26
9	32.7	63
12	48.89	122

Since the mass of glass slide is greater than the coverslip, more heat and hence more current is needed to generate the same temperature change, ΔT. In other words, coverslip generates more temperature rise at the same current compared to glass slide. Since, in the current work a final temperature of 70 °C on the surface us required, from Figure 3.13, it corresponds to a 10 mA for glass slide and 8mA for coverslip . As the difference in current is not much for lower temperatures, glass slide was selected because of its ease of handling

Figure 3.13 shows the comparison of temperature variation in case of glass slide and coverslip. It is clear that for the same current, higher temperature change is observed for the cover slip compared to glass slide.

.

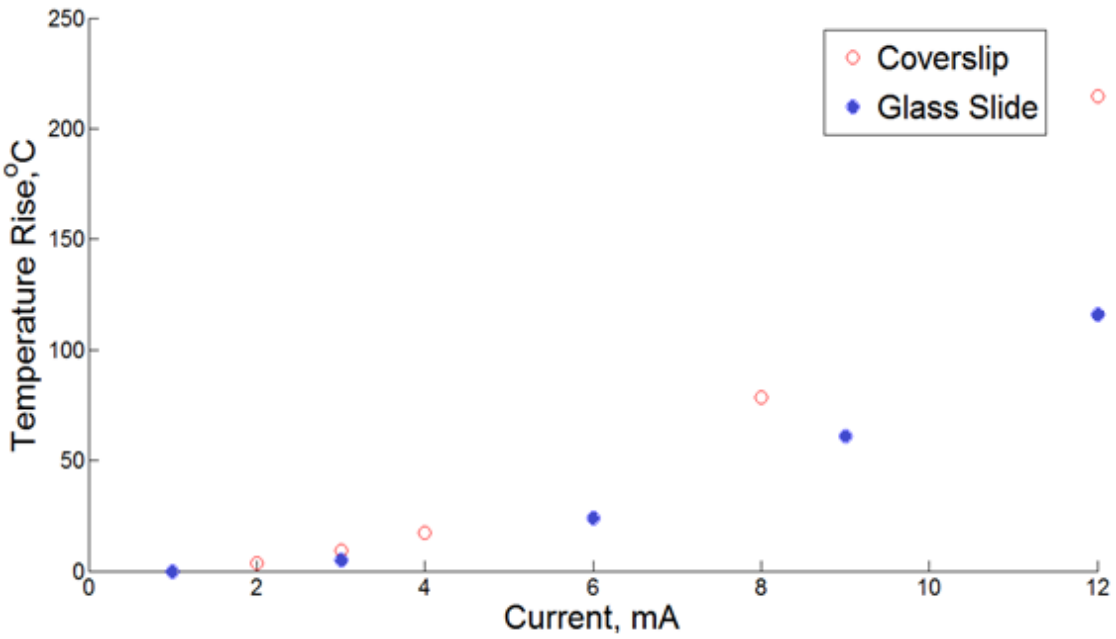

Figure 3.13: Current vs Temperature curve for Glass Slide and Cover Slip

If higher temperature rise is desirable at a comparatively lower current, coverslips can be used instead of glass slides.

CHAPTER 4

SPECIFIC DETACHMENT OF DNA

This chapter discusses an application of Micro heater device for specific detachment of DNA. In the past few decades, a lot of research has been done to immobilize DNA on a solid surface and for DNA detection. Different types of techniques have been designed to detect DNA at ultra-low concentration. With the innovation in nanowires and carbon nanotubes, the selectivity and sensitivity of the DNA sensors has increased multiple times. Surface functionalization has always acted as a bridge for these types of chemistries and sensing techniques. There are a number of techniques to immobilize DNA on a solid surface. The focus of the current experiments was to specifically detach DNA from certain areas of a glass substrate by manipulating the surface chemistry using thermal input. Different techniques to immobilize DNA will be dicussed. A detailed procedure followed to design and functionalize the glass slide with micro heater device will be highlighted. The experimental setup and results will be discussed.

4.1 Materials and Methods

4.1.1 Chemicals and Biomolecules Used

The chemicals and biomolecules used in this recipe include 3-Amminopropyltriethoxysilane (APTES), NHS-Biotin, BSA, FITC-Streptavidin, Toluene, DimethylSulfoxide (DMSO), 10X PBS and Biotinylated DNA.

4.1.2 Design

A number of techniques have been developed to characterize the surface chemistry and topography. These include FTIR, EDS, Raman Spectroscopy and AFM, etc. Fluorescent microscopy is the easiest approach to confirm the presence of biomolecules on a surface. In

order to confirm the functionalization and immobilization of DNA, fluorescent microscopy was used. To confirm the presence of streptavidin on the NHS biotin modified surface, FITC was used as fluorescence. FITC has excitation and emission spectrum peak wavelengths of approximately 495 nm and 521 nm respectively. It emits green fluorescence upon excitation (Filter 2 in Meiji 6300 microscope). To confirm the presence of biotinylated DNA, Texas Red flourophore was used on 3' end of the biotinylated DNA. Texas Red fluoresces in 615 nm range, and the peak absorption spectrum is observed at 589 nm (Filter 5 in meiji 6300 microscope in lab). DNA sequence used for this experiment was 3'-biotin-AGT TCA TAT GGGC C-Texas Red-5'. The goal was to raise the temperature of the heater to 70 C by applying current, introduce non- ionic aqueous solution on the surface and help the bonds between streptavidin and biotin (attaché dto DNA) near the microheater to break under the influence of heat and resulting into no fluorescence near microheater as biotinylated DNA is detached.

4.1.3 Preparation of Glass slide:

The glass slides from Fisher Scientific were first used to fabricate the micro heater. The devices were then immersed in ethanol for 10 minutes followed by rinsing with DI water and dried under nitrogen. The glass slides were then heated on a hot plate for 3 minutes at 80 C to remove any moisture and keep aside to cool down and then stored in petri dishes before further use.

4.1.4 Surface functionalization to immobilize DNA

The DNA was immobilized on the surface using the techniques described elsewhere [77- 78]. A PDMS well was created around the heater line and micropipettes were used for the step by step application and washing of different chemicals/biomolecules as described in the functionalization protocol below. The glass slide with micrometer device was aminomodified by incubation in 2.0 mM aminopropyltriethoxysilane(APTES), from Sigma-Aldrich, for 1 h at room temperature. The APTES solution was prepared using toluene as the solvent. The incubation was followed by three washes in toluene and one in DI water. The amino groups were coupled

to biotin by incubation in 3.4 mM NHS-biotin for 1 h at room temperature; the NHS-biotin was prepared using dimethyl sulfoxide (DMSO) as the solvent. This was followed by three washes in DMSO and one in DI water to remove any DMSO traces. After NHS-biotin deposition, the sample was immersed in1% BSA solution in PBS for 1 h. The main purpose of BSA coating is to block any uncovered portion of glass. These BSA molecules do not exhibit any interactions with either biotin or streptavidin .Binding of FITC-streptavidin was carried out by incubation in 1 μM streptavidin for 30 min followed by washing with phosphate-buffered saline (PBS). Biotinylated DNA oligonucleotides were applied to the surface for 30 min before washing with PBS. Figure 4.1 (a) shows the schematic of the complete recipe.

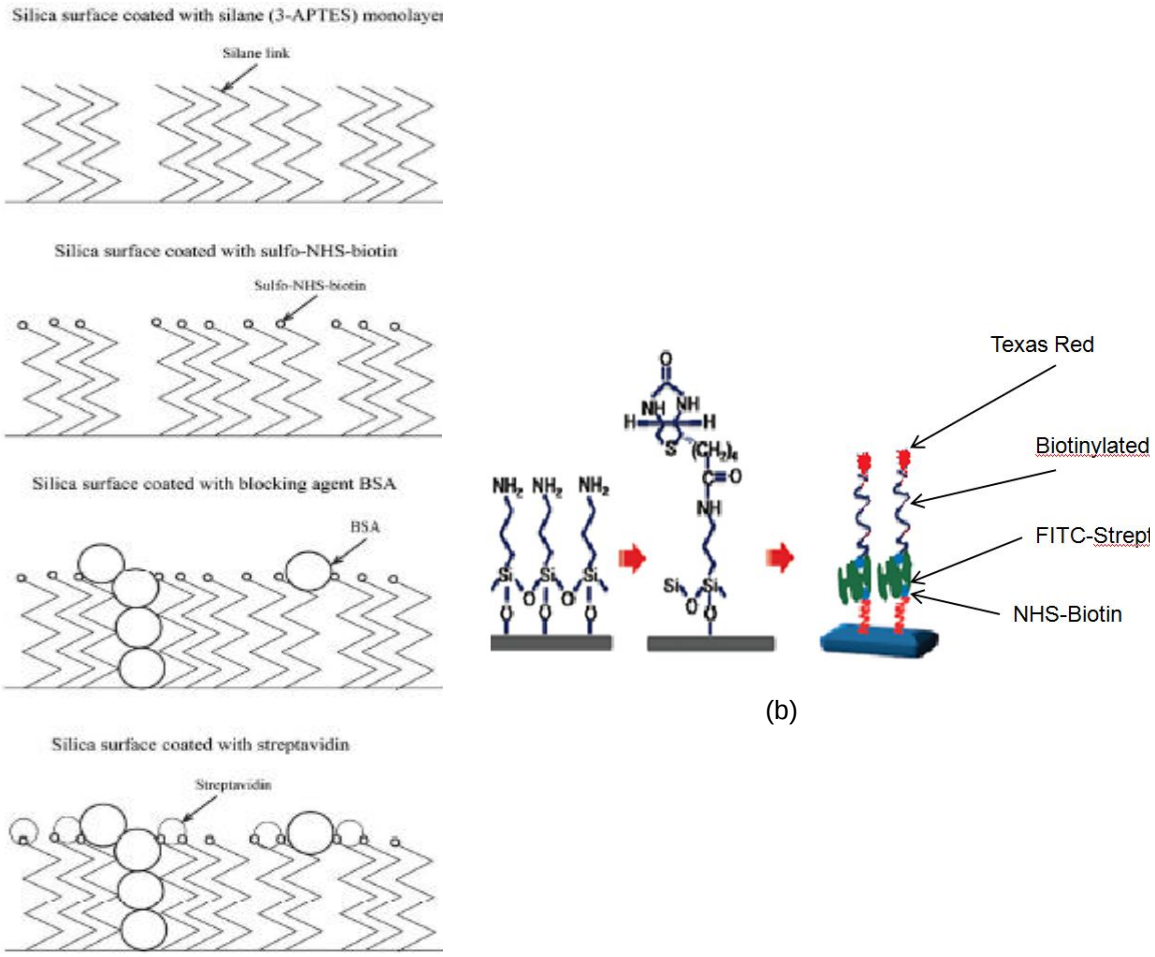

Figure 4.1: (a) Schematic of DNA immobilization technique [78] (b) Immobilization by the Biotin-Streptavidin Interaction with fluorescent labels [77]

4.2 Experimental Setup and Results

4.2.1 Without BSA

For the first set of experiments for the surface functionalization, BSA was not used which means that the uncovered portion of the SAM is exposed to streptavidin. This resulted into non-specific binding of Streptavidin on glass surface and streptavidin was nonspecifically coated on all over the area of interest. This resulted into green fluorescence all over the functionalized area as shown in Figure 4.2 (a). Bitonylated DNA was immobilized on this

streptavidin coated area using the recipe discussed in section 4.3.3. Fluorescent images were taken. DNA was bound all over the streptavidin coated area as expected as shown in Figure 4.4 (b)

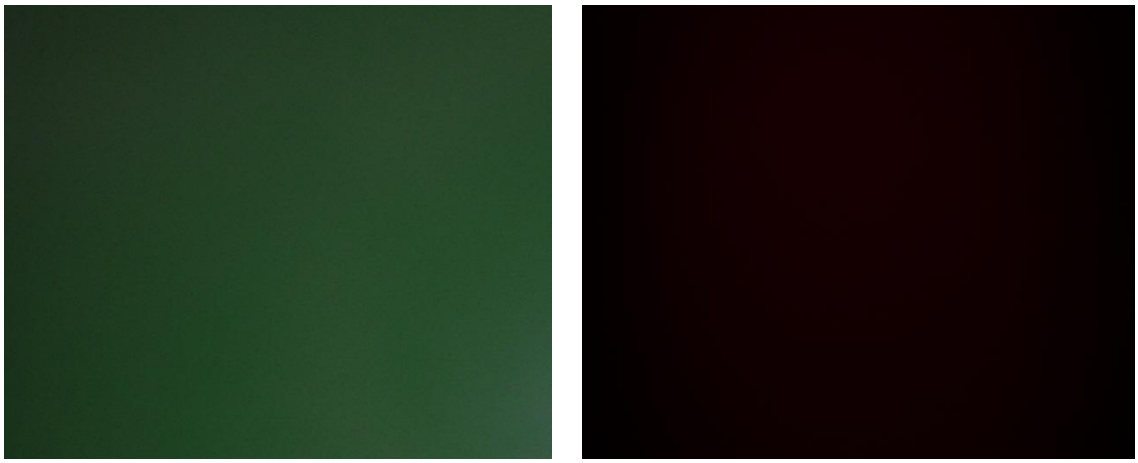

(a) (b)

Figure 4.2: (a) FITC-Streptavidin Coated glass slides without application of BSA (b) The resulting DNA attachment

4.2.2 With BSA

In the second experiment, BSA was used before application of streptavidin to make sure that all the uncovered (without SAM) areas on glass are blocked. Figure 4.3 shows the resulting fluorescent images for FITC streptavidin and immobilized DNA.

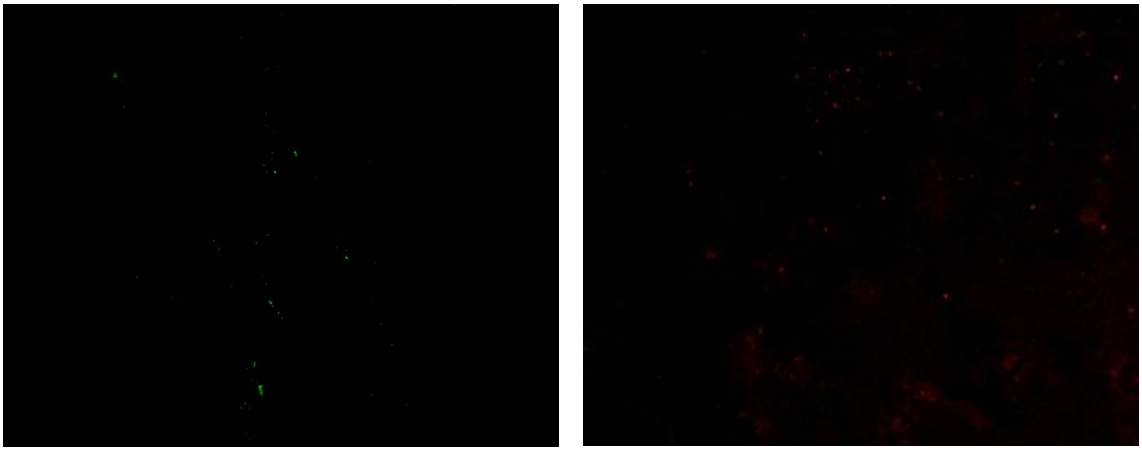

(a) (b)

Figure 4.3: (a) FITC-Streptavidin Coated glass slides application of BSA (b) The resulting DNA attachment

As can be seen from Figure 4.2 and 4.3, there is fluorescence all over the surface when no BSA was used. When BSA was used the green fluorescence of FITC-streptavidin and corresponding red fluorescence of DNA was observed on specific regions.

To confirm that streptavidin and DNA are immobilized as a result of covalent bonding, two slides were prepared. One was functionalized with streptavidin only and the other functionalized to the final step of immobilizing DNA. Both slides were washed thoroughly with DI water and observed under the microscope. The wash was collected ad observed under the microscope. No fluorescence was observed from the wash.

4.2.3 Application of Heat Using Micro heater on DNA Immobilized Chip

In 2005, Holmberg *et al* showed that biotin-streptavidin bond can be broken by using aqueous solution at 70 °C and exposing for seconds [79]. This technique was used to break this bond and hence detach DNA from the surface. The DNA immobilized surfaces were heated using the micro heater. In order to do so, direct connections to the contact pads were made. Nonionic aqueous solution was applied through the PDMS gasket and current was raised from 1-10mA to get the expected resistance value of 3700 Ohms which corresponds to 70-75 °C.

The current was applied for varying durations of 30 seconds, 60 seconds and 90 seconds.. Figure 4.4 shows the fluorescent images taken before the application of heat. As it can be seen the particles and hence the fluorescence is all over the functionalized area. The heater line is hidden behind the fluorescence. Keeping the microscope at the same point, when current was applied the number of particles close to heater line reduced by a large scale as expected. This fact can be seen from Figure 4.5.

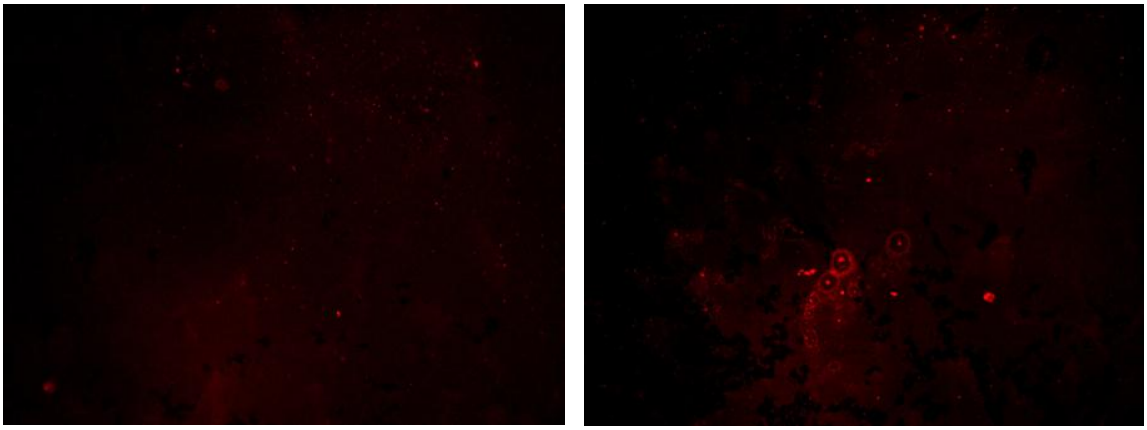

Figure 4.4: Before Heating slides with Immobilized DNA

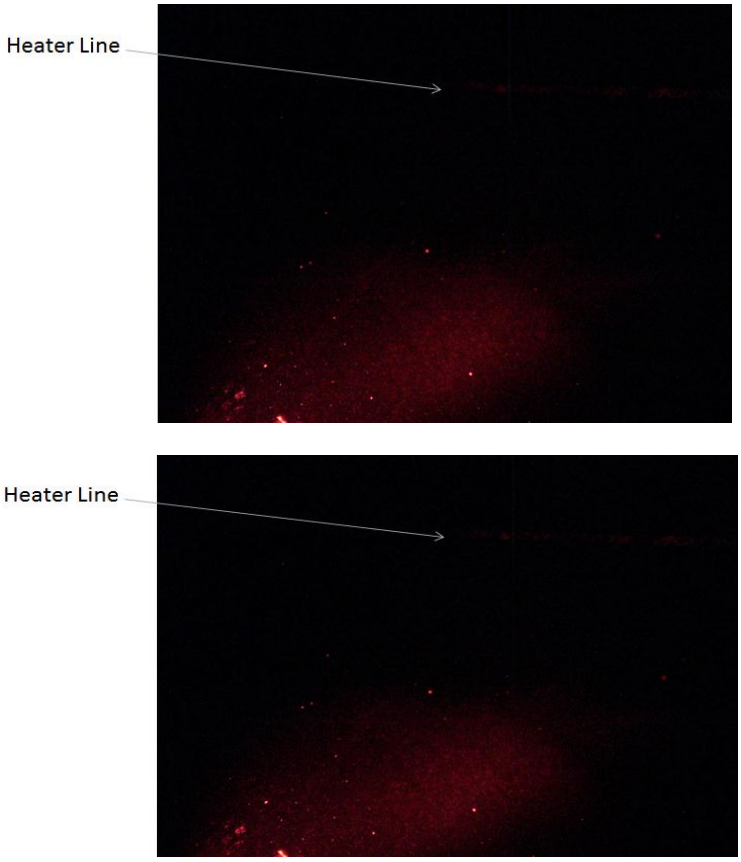

Figure 4.5: After heating slides with Immobilized DNA using microheater device from two experiments

CHAPTER 5

CONCLUSIONS AND FUTURE WORK

5.1 Conclusions

This thesis described the fabrication of a micro heater device for controlled heat generation in order to manipulate biomolecules such as DNA. Thermal calibration and characterization of the device was done in a controlled environment. Finite-element simulations were carried out to characterize and compare the results with the experimental data. Experimental data showed excellent agreement with simulation results. As an application of the microheater device, investigation of DNA detachment from a glass surface based on disruption of the Biotin-Streptavidin chemical bond was carried out. Results obtained throw light on this interesting phenomena and offer interesting pathways for further investigation in the future.

5.2 Future Work

This section highlights a few possible applications of the microheater described in this work and related future research directions.

5.2.1 Microbubble Generation using Microheater

Microheater devices can be used to generate microbubbles in different solutions. The heat generated by these devices can help in producing size-controlled microbubbles which have significant potential applications in several areas of engineering and biomedicine. The most successful application for thermal bubbles is the ink-jet printer, where tiny droplets are ejected by the power of thermal bubbles at a very high frequency for printing [84]. Recently, new technologies have led to advances in the manufacturing of ink-jet printer heads. For example, fabrication processes s have improved dramatically since the early ink-jet printers were introduced [80-84]. Many different types of applications are currently under investigation.

For example, microbubbles have also been used to move microstructures laterally in a micro steam engine [85]. In other applications, microbubbles have been proposed to expel liquid as pumping sources or mechanical valves in micromachined flow channel shows a cross-sectional view of a microchannel that was fabricated by a surface micromachining process. It would be interesting to generate microbubbles using the microheater device described here for the applications described above.

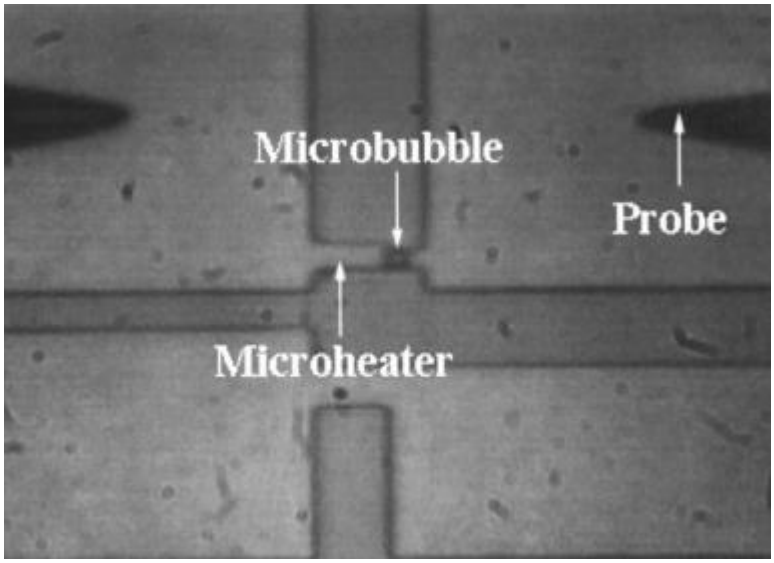

Figure 5.1: A single Micorbubble with 2 uM diameter generated using a Microheater [86]

5.2.2 Microheaters for Digital Microfluidics (DMF) and Cell Manipulation

Microheater designed can be used for a number of applications in microfluidics and cell manipulation. These include Cell lysing, cell patterning using micro-heater controlled thermoresponsive thin films.

DMF is an attractive platform for biological applications, which often require the use of expensive or precious reagents. However, a nontrivial challenge in the implementation of DMF for such applications is nonspecific adsorption by biological molecules. This phenomenon can lead to sample loss and cross contamination, and even more troubling, it can promote droplet sticking, which renders devices useless. In an important step toward overcoming this problem,

in 2004, Srinivasan et al [87] demonstrated that fouling could be minimized by suspending droplets in an immiscible oil; this technique facilitated manipulation of a variety of fluids containing high concentrations of potential surface-fouling molecules, including blood, serum, plasma, and tear. These type of DMF based chips have applications ranging from DNA extraction, repair and amplification to Proteomics [88-91] and cell assays [92-94].

5.2.3 Separation of DNA based on Length

DNA of various lengths behaves differently at the same temperature. Since using this device, a temperature profile can be generated along the surface, it can be used to separate DNA based on their lengths.

REFERENCES

1. Bashir R., *Adv. Drug Del. Rev.*, 56, 1565—1586 (2004).
2. Grayson, A. C. R.; Shawgo, R. S.; Johnson, A. M.; Flynn, N. T.; Li,Y. W.; Cima, M. J.; Langer, R. A BioMEMS review: MEMStechnology for physiologically integrated devices. Proc. IEEE 2004,92 (1), 6-21
3. Serrell DB, Oreskovic TL, Slifka AJ, Mahajan RL, Finch DS. A uniaxial bioMEMS device for quantitative force-displacement measurements. *Biomed Microdevices* 9:267–275, 2007
4. Service, R. F. Science 1998, 282, 396
5. Ramsay, G. Nature Biotech. 1998, 16, 40.
6. Dai, C.L. A capacitive humidity sensor integrated with micro heater and ring oscillator circuit fabricated by CMOS-MEMS technique. Sens. Actuat. B 2007, 122, 375-380.
7. Sberveglieri, G.; Hellmich W.; Müller, G. Silicon hotplates for metal oxide gas sensor elements. Microsystem Technologies, 1997, 3, 183.
8. Chen, L.; Mehregany, M. Exploring silicon carbide for thermal infrared radiators. In Proceedings of the 6th IEEE Sensors Conference, Atlanta, GA, USA, 28–31 October 2007; pp. 620-623.
9. Wilchek M, Bayer EA, eds. Methods of enzymology. Vol. 184. New York: Academic Press, 199.
10. Mailly, F.; Giani, A.; Bonnot, R.; Temple-Boyer, P.; Pascal-Delannoy, F.; Foucaran, A.; Boyer, A. Anemometer with hot platinum thin film. Sens. Actuat. A 2001, 94, 32-38.
11. Dai, C.L. A capacitive humidity sensor integrated with micro heater and ring oscillator circuit fabricated by CMOS-MEMS technique. Sens. Actuat. B 2007, 122, 375-380.
12. Chen, L.; Mehregany, M. Exploring silicon carbide for thermal infrared radiators. In Proceedings of the 6th IEEE Sensors Conference, Atlanta, GA, USA, 28–31 October 2007; pp. 620-623.
13. Aslam, M.; Gregory, C.; Hatfield, J.V. Polyimide membrane for micro-heated gas sensor array. Sens. Actuat. B 2004, 103, 153-157.
14. Mo, Y.W.; Okawa, Y.; Tajima, M.; Nakai, T.; Yoshiike, N.; Katukawa. Micro-machined gas sensor array based on metal film micro-heater. Sens. Actuat. B 2001, 79, 175-181.
15. Tao, C.; Yin, C.; He, M.; Tu, S. Thermal analysis and design of micro-hotplate for Si-substrated micro-structural gas sensor. In Proceedings of the 3rd IEEE International Conference on Nano/Micro Engineered and Molecular Systems, Sanya, China, 6–9 January 2008; pp. 284-287.

16. Das, N.C.; Jhabvala, M.; Robinson, D.; Shu, P. Low power polysilicon sources for IR applications. In Proceedings of 5th International Conference on Solid-State and Integrated Circuit Technology, Beijing , China, 21–23 October 1998; pp. 884-886.

17. Moseley, P.T.; Norris, J; Williams, D.E. Techniques and Mechanisms in Gas Sensing, Adam Hilger, Bristol, Philadelphia and New York, 1991.

18. Wöllenstein, J.; Böttner, H.; Jaegle, M.; Becker, W.J.; Wagner, E. Material properties and the influence of metallic catalysts at the surface of highly dense SnO2 films. Sensors & Actuators B, 2000, 70, 196.

19. Bârsan, N. Fundamental and practical aspects in the design of nanoscaled SnO2 gas sensors: a status report. Fresenius J. Anal. Chem., 1999, 365, 287.

20. Müller, G.; Friedberger, A.; Kreisl, P.; Ahlers, S.; Schulz, O.; Becker, T. A MEMS toolkit for metal-oxide-based gas sensing systems. Thin Solid Films, 2003, 436, 34.

21. Sberveglieri, G.; Hellmich W.; Müller, G. Silicon hotplates for metal oxide gas sensor elements. Microsystem Technologies, 1997, 3, 183.

22. Heilig, A.; Barsan, N.; Weimar, U.; Göpel, W. Selectivity enhancement of SnO2 gas sensors simultaneous monitoring of resistances and temperatures. Sensors & Actuators B, 1999, 58, 30. Sensors 2006, 6 418

23. Brand, D.; Krauss, A.; van der Schoot, B.; Weimar, U.; Bârsan, N.; Göpel, W.; de Rooij, N.F. Design and fabrication of high-temperature micro-hotplate for drop-coated gas sensors. Sensors & Actuators B, 2000, 68, 223.

24. Gardner, J.W.; Bartlett, P.N. Electronic noses: Principles and applications, Oxford University Press, 1999.

25. Gardner, J.W.; Lee, S.M.; Bartlett, P.N.; Guerin, S.; Briand, D.; de Rooij, N.F. Silicon planarmicrocalorimeter employing nanostructured films. Transducers 2001, Germany, Munich, Germany, June 10-14, 2001.

26. Kreisl, P.; Helwig, A.; Müller, G.; Obermeier, E.; Sotier, S. Detection of hydrocarbon species using silicon MOS field-effect transistors operated in a non-stationary temperature-pulse mode. Sensors & Actuators B, 2005, 106, 442.

27. 11. Lobert, P.E.; Bourgeois, D.; Pampin, R.; Akheyar, A.; Hagelsieb, L.M.; Flandre, D.; Remacle, J. Immobilization of DNA on CMOS compatible materials. Sensors and Actuators B, 2003, 92, 90.

28. Stankova, M.; Ivanov, P.; Llobet, E.; Brezmes, J.; Vilanova, X.; Gràcia, I.; Cané, C.; Hubalek, J.; Malysz K.; Correig, X. Sputtered and screen-printed metal oxide-based integrated micro-sensor arrays for the quantitative analysis of gas mixtures. Sensors and Actuators B, 2004, 103, 23.

29. Solzbacher, F.; Imawan, C.; Steffes, H.; Obermeier, E.; Eickhoff, M. A new SiC/HfB2 based low power gas sensor. Sensors and Actuators B, 2001, 77, 111.

30. Pollien, A.; Baborowski, J.; Ledermann, N.; Muralt, P. New Material for thin film filament of micromachined hot-plate. Transducers 2001, Munich, Germany, June 10-14, 2001.

31. Yuasa, H.; Ohya, S.; Karasawa, S.; Akimoto, K.; Kodato, S.; Takahashi, K. Single crystal silicon micromachined pulsed infrared light source, Transducers 1997, Chicago, June 16-19, 1997.

32. Ohlckers, P.; Ferber, A.M.; Dmitriev, V.K.; Kirpilenko, G. A photo-acoustic gas sensing silicon microsystem. Transducers 2001, Germany, Munich, Germany, June 10-14, 2001.

33. Luthardt, M. Ein flammenloser Ionisationsdetektor, CLB Chemie in Labor und Biotechnik, 48. Jahrgang, Heft 5, 1997.

34. Rasulev, U.Kh.; Nazarov, E.G.; Khudaeva, G.B. Chromatographic determination of trace amounts of amines using surface ionization detector. Journal of Chromatography A, 1995, 704, 473.

35. Wolf, S.; Tauber, R. N. Silicon Processing for the VLSI Era; Lattice Press: Sunset Beach, 1986

36. Haefliger, D., Stemmer, A., Mikrolithographie ohne Reinraum und Vakuum, Technische Rundschau, 7, 2002, 26-27

37. http://snf.stanford.edu/Process/Lithography/liftoff.html

38. Shinwari, M.W.; Deen M.J.; Landheer, D. Study of the electrolyte-insulator-semiconductor fieldeffect transistor (EISFET) with applications in biosensoe design. *Microelectron. Reliab.* 2007, *47*, 2025-2057.

39. Xu J, Luo Xi-Liang, Chen Hong-Yuan. Analytical aspects of FETbasedbiosensors. Frontiers Biosci 2005;10:420–30.

40. Sakata T, Kamahori Masao, Miyahara Yuji. Immobilization of oligonucleotide probe on Si3N4 surface and its application to generic field effect transistor. Mater Sci Eng C 2004;24:827–32

41. Peterson AW, Heaton Richard J, Georgiadis Rosina M. The effect ofsurface probe density on DNA hybridization. Nucleic Acids Res2001;29(24):5163–8.

42. Souteyrand E et al. Direct detection of the hybridization of synthetichomo-oligomer DNA sequences by field effect. J Phys Chem B1997;101:2980–5.

43. Y. J. Oh, W. Jo, J. A. Kim and S. Park, J. Korean Phys. Soc. 48, 1642 (2006).

44. S. Kim, T. W. Kwon, J. Y. Kim, H. Shin, J. G. Lee and M. M. Sung, J. Korean Phys. Soc. 49, 736 (2006).

45. Bishop, A.R.; Nuzzo, R.G. Current Opinion in Colloid and Interface Science 1996

46. Ulman, A. Formation and Structure of Self-Assembled Monolayers. Chem. Rev. 1996, 96, 1533-1554

47. Bigelow, W. C.; Pickett, D. L.; Zisman, W. A. J. Colloid Interface Sci. 1946, 1, 513.

48. Tirrell, D. A.; et al. MRS Bull. 1991, July, 23-28.

49. Love *et al*; Estroff, Lara A.; Kriebel, Jennah K.; Nuzzo, Ralph G.; Whitesides, George M. (2005). "Self-Assembled Monolayers of Thiolates on Metals as a Form of Nanotechnology". Chem. Rev. 105 (4): 1103–1170.

50. Vos, Johannes G., Robert J. Forster, Tia E. Keyes (2003). Interfacial Supramolecular Assemblies. Wiley. pp. 88–94.

51. adou, Marc (2002). Fundamentals of Microfabrication: The Science of Miniaturization. CRC. pp. 62–63

52. Saliterman, Steven (2006). Self-assembled monolayers (SAMs). Fundamentals of BioMEMS and Medical Microdevices. SPIE Press. pp. 94–96.

53. Bucher, Jean-Pierre; Santesson, Lars, Kern, Klaus (31 March 1994). "Thermal Healing of Self-Assembled Organic Monolayers: Hexane- and Octadecanethiol on Au(111) and Ag(111)".Langmuir 10 (4): 979–983. doi:10.1021/la00016a001.

54. Schlenoff, Joseph B.; Li, Ming, Ly, Hiep (30 November 1995). "Stability and Self-Exchange in Alkanethiol Monolayers". Journal of the American Chemical Society 117 (50): 12528–12536.doi:10.1021/ja00155a016

55. Wong, J.; Chilkoti, A.; Moy, V. T. *Biomol. Eng.* 1999, *16*, 45-55.

56. Merck Index, 11th edition 1244

57. Weber, et al.Science 6 January 1989: 85-88.DOI:10.1126/science.2911722

58. Green, NM (1975). "Avidin". *Advances in protein chemistry* 29: 85–133

59. Kraulis, P.J., J. Appl. Cryst. 1991, 24, 946

60. Livnah, O; Bayer, EA; Wilchek, M; Sussman, JL (1993). "Three-dimensional structures of avidin and the avidin-biotin complex". *Proceedings of the National Academy of Sciences of the United States of America.* 90(11):5076–80

61. Wilchek M, Bayer EA. Biotin-containung reagents [Review].MethodsEnzymol 1990;184:123-38.

62. Guesdon JL, Ternynck T, Avrameas S. The use of the avidinbiotin interaction in immunoenzymatic techniques. J Histochem Cytochem 1979;27:1131-9.

63. Fehskens E, Burgett MW. Measurement of serum chorionic gonadotropin by a biotin-avidin labeled enzyme immunoassay. Ann Clin Lab Sci 1985;15:241-5

64. Mouton CA, Pang D, Natraj CV, Shater JA. A reagent for covalently attaching biotin to proteins via a cleavable connector arm. Arch Biochem Biophys 1982;218:1O1-8.

65. Shimkus M, Levy T, Herman T. A chemically cleavable biotinylated nucleotide: usefulness in the recovery of protein-DNA complexes from avidin affinity columns. Proc NatI Acad Sci USA 1985;82:2593

66. Gretch DR. Suter M, Stinski MF. The use of biotinylated monoclonal antibodies and streptavidin affinity chromatography of isolated Herpesvirus hydrophobic proteins or glycoproteins. Anal Biochem 1987;163:270-7.

67. Ghebrehiwet B, Bossone S. Reversible biotinylation of Clq with a cleavable biotinylated derivative. Application in Clq receptor (ClqR)purification. J Immunol Methods 1988;110:251-60

68. Moseley, P.T.; Norris, J; Williams, D.E. Techniques and Mechanisms in Gas Sensing, Adam Hilger, Bristol, Philadelphia and New York, 1991.

69. Wöllenstein, J.; Böttner, H.; Jaegle, M.; Becker, W.J.; Wagner, E. Material properties and the influence of metallic catalysts at the surface of highly dense SnO2 films. Sensors & Actuators B, 2000, 70, 196

70. Mo, Y.W.; Okawa, Y.; Tajima, M.; Nakai, T.; Yoshiike, N.; Katukawa. Micro-machined gas sensor array based on metal film micro-heater. Sens. Actuat. B 2001, 79, 175-181

71. Müller, G.; Friedberger, A.; Kreisl, P.; Ahlers, S.; Schulz, O.; Becker, T. A MEMS toolkit for metal-oxide-based gas sensing systems. Thin Solid Films, 2003, 436, 34

72. P.K Dixon an S.R Nagel, *Phy. Rev. lett*. 61,341 (1988)

73. Glassbrenner, C.J. & Slack, G.A. Thermal Conductivity of Silicon and Germanium from 3 K to the Melting Point. Physical Review 134, A1058 (1964)

74. Young, Hugh D., University Physics, 7th Ed., Addison Wesley, 1992.

75. Thermal conductivity 21, Clifford J. Cremers, H. Alan Fine, H. 1990.

76. J. R. Black, IEEE Trans. Electron Devices ED-16~4!, 338 ~1969!.

77. Kasry, A.; Borri, P.; Davies, P. R.; Harwood, A.; Thomas, N.;Lofas, S.; Dale, T. ACS Appl. Mater. Interfaces 2009, 1, 1793–1798

78. Bhushan B, Tokachichu D.R, Keener M.T, Lee S.C Nanoscale adhesion, friction and wear studies of biomolecules on silicon based surfaces. Acta Biomater. 2, 2006a 39–49

79. A. Holmberg, A. Blomstergren, O. Nord, M. Lukacs, J. Lundeberg, M. Uhlen, Electrophoresis 2005, 26, 501

80. R. Askeland, W. Childers, and W. Sperry, The Second Generation Thermal Inkjet Structure, HP Jou rnal, pp. 376]384, August 1988.

81. J. S. Aden, J. H. Bohorquez, D. M. Crook, A. Gacia, and U. E. Hess, The Third Generation Thermal Inkjet Structure , HP Journal, pp. 41]45, February 1994.

82. C. C. Beatty, A Chronology of The rmal Ink-Jet Structure s, Techn ical Digest of IEEE Solid -State Sensor an d Actu ato r Workshop, pp. 200]204, June 1996.

83. D. Westberg and G. I. Andersson, A Nove l CMOS-Compatible Inkje t Head, Digest of Transducers ’97, Int. Co nf. o n Solid -State Sen sors an d Actu ato rs, pp. 813]816, 1997

84. N. J. Nie lsen. History of Thinkjet Printerhead Deve lopment, HP Journal, vol. 36, no. 5,pp. 4]10, 1985

85. J. J. Sniegowski, A Micro Actuation Mechanism Based on Liquid-Vapor Surface Tension, Digest of Late News of Transducers ’93, Int. Conf. on Solid -State Sensors and Actuators, pp. 12]13, 1993

86. Lin, L. W., Microscale Thermophys. Eng. 1998, 2, 71–85

87. V. Srinivasan, V. K. Pamula, R. B. Fair, Lab Chip 2004, 4, 310

88. A. R. Wheeler, H. Moon, C. J. Kim, J. A. Loo, R. L. Garrell, Anal. Chem. 2004,76, 4833.

89. A. R. Wheeler, C. A. Bird, J. A. Loo, R. L. Garrell, R. R. O. Loo, C. J. Kim, H.Moon, Anal. Chem. 2005, 77, 534.

90. T. Taniguchi, T. Torii, T. Higuchi, Lab Chip 2002, 2, 19.

91. E. M. Miller, A. R. Wheeler, Anal. Chem. 2008, 80, 1614.

92. Barbulovic-Nad, H. Yang, P. S. Park, A. R. Wheeler, Lab Chip 2008, 8,519.

93. J. Zhou, L. Lu, K. Byrapogu, D. M. Wootton, P. I. Lelkes, R. Fair, Virtual Phys.Prototyping 2007, 2, 217.

94. S.-K. Fan, P.-W. Huang, T.-T. Wang, Y.-H. Peng, Lab Chip 2008, 8, 1325

BIOGRAPHICAL INFORMATION

Annas Javed was born in Lahore, Pakistan, in August, 1986. He finished his schooling in his hometown and did his undergraduate studies from University of Engineering and Technology, Lahore Pakistan in Electrical Engineering. He joined UTA in Spring 2010. He is interested in pursuing a PhD in the area of BioMEMS and Targeted Drug Delivery. Towards this goal, he joined Dr. Ankur Jain's group at UTA in August 2011. Here, he has identified a novel technique to selectively detach DNA from the surface.